BIOENGINEERING

Bacteria give nanoparticles a ride

Bacteria are useful targeted delivery agents and nanoparticles are efficient transporters of plasmid DNA. Now, a hybrid of the two will improve strategies to transfect cells for vaccination and cancer treatment.

Guido Dietrich
is at Berna Biotech AG, 3018 Berne, Switzerland.
e-mail: guido.dietrich@bernabiotech.com

Vaccination has proven to be the most cost-effective medical strategy for preventing infectious diseases. To mimic a natural infection, genetically modified live pathogens, such as viruses or bacteria, are introduced into the body. Although they are too weak to cause a clinical disease or the side effects of wild-type viruses and bacteria, these attenuated pathogens can still trigger a self-limiting infection that stimulates the production of antibodies. Such vaccines are currently used worldwide to prevent diseases like measles, mumps, rubella, polio, tuberculosis and typhoid fever.

An outgrowth of vaccination was the idea to use attenuated bacteria as 'carriers' to transport plasmid DNA to the nuclei of specific cells. This so called 'bactofection' can stimulate the production of antibodies from a wide variety of pathogens[2,3] by releasing plasmid DNA specifically encoded to stimulate the production of a particular antigen, and could even serve as a general vaccination against cancer[5,6]. Attenuated bacteria like *Shigella*[2], *Salmonella*[3] and *Listeria*[4] have all been used as bactofection delivery agents.

One of the major obstacles for bactofection is transferring the plasmid DNA from inside the bacteria to the host cell. Usually this process requires that the bacteria first break up and release the plasmid molecules[2,4]. In contrast, nanoparticles coated with plasmid DNA are more effective at delivering their cargo, provided they can be targeted to reach the appropriate host-cell nucleus. Now, as reported today on the *Nature Nanotechnology* website, in a clever combination of microbiology and nanotechnology, biologists and engineers at Purdue University are using bacteria for the delivery of plasmid-coated nanoparticles[1], which should enhance the efficiency of bacteria as delivery systems and enable the specific targeting of nanoparticles to human cells.

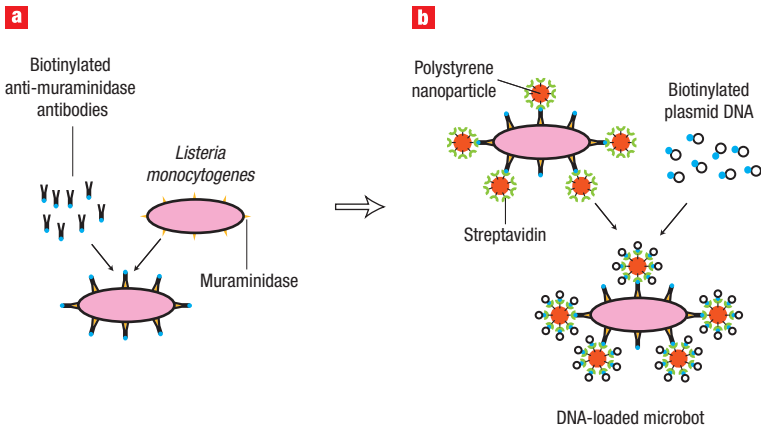

Figure 1 Steps in generating bacterial microbots. **a**, Antibodies that contain biotin (solid blue circles) bind to muraminidase proteins on the surface of the bacteria *L. monocytogenes*. **b**, The bacteria are then mixed with nanoparticles (red) that have been coated with strepatavidin (green), a molecule that binds strongly to biotin. The remaining free streptavidin molecules on the nanoparticles are then coupled to plasmid DNA (black circles) that carry biotin to create functional microbots.

The Purdue team, led by Rashid Bashir, coupled polystyrene nanoparticles loaded with plasmid DNA to the surface of attenuated *Listeria monocytogenes* bacteria. Three steps were necessary to make these hybrids that the group calls 'microbots' (Fig. 1). The group first treated the bacteria with a biotin-carrying antibody that acts against — and will therefore attach to — proteins on the bacterial surface called muraminidase. Next, they mixed the treated bacteria with nanoparticles coated with streptavidin, a protein that binds strongly to biotin. Finally, the nanoparticle-loaded bacteria were mixed with plasmid DNA carrying biotin, which binds to the free strepdavidin sites on the surface of the nanoparticles.

The *L. monocytogenes* bacteria are about 1 µm in length and using the microbot procedure it is possible to attach nanoparticles ranging in size from 40–200 nm to the bacterial surface. Interestingly, only one to three of the 200 nm particles can bind to a single bacterium, much less than one would expect for perfect coverage, whereas the loading capacity seems to be considerably higher for the 40 nm particles.

Because the microbots carry the nanoparticles on their surface, the plasmid DNA coupled to the nanoparticles can access the interior of the host cells much more smoothly than with conventional bactofection strategies. Using *L. monocytogenes* as the carriers also has an important benefit. Most bacteria are swallowed up and killed in the 'vacuoles' of specialized cells of the immune system (like macrophages). In contrast, *L. monocytogenes* can form pores in the vacuole membranes which allow them to escape and provide the nanoparticle with access to the interiors — and importantly, the nuclei — of virtually all kinds of human cells.

To confirm that the host cells express the desired plasmid-encoded antigens, the nuclei of several types of human cell lines were first targeted to express the easily detected green fluorescent protein (GFP). *In vitro*, the microbots are able to transfect between 2 and 20% of the cells — a notable

efficiency, given that nanoparticles alone are not able to transfect the human cells. Using another model antigen (firefly luciferase), *in vivo* studies of mice were performed, which showed that the microbots can even be used to transfect entire organs. Although the microbots exhibit some cytotoxicity for their target cells, owing to their bacterial nature, the effects are surprisingly milder than nanoparticles alone.

Despite the success of this initial step, quite a bit of work is still necessary. First, after delivering model antigens like GFP and the firefly luciferase, real antigens from pathogenic bacteria and viruses should now be delivered by microbots. However, another major concern is that the *L. monocytogenes* strain used by the Bashir group was a wild-type strain, which is lethal for mice and required that they be treated with antibiotics. Although diseases caused by *L. monocytogenes* are rare in humans, the fact that this bacteria is able to infect virtually all human organs and cell types means it can cause encephalitis, meningitis and sepsis, particularly in immuno-compromised individuals.

These safety issues could be addressed by using attenuated strains of *L. monocytogenes* that target host cells with greater specificity. Although such strains are available[4,8], one of which was recently shown to be quite safe in a phase 1 clinical trial[8], they are still not sufficiently targeted for a particular organ or type of host cell to be considered safe.

An alternative would be to use bacteria that have already been approved for human use, such as the vaccine strains for tuberculosis (*Mycobacterium bovis* BCG) and typhoid fever (*Salmonella typhi* Ty21a), both of which have surface proteins that can serve as docking stations for nanoparticles. Although these bacteria tend to become trapped in the host-cell vacuole, equipping them with listeriolysin provides them with the same ease of escape as the *L. monocytogenes* in the microbots[9].

The microbots open novel avenues for nanoparticle researchers, as the delivery of substances other than DNA should be possible. For example, microbots may be useful in the targeted delivery of molecules such as hormones, enzymes, toxins and small inhibitory RNAs for therapeutic interventions. In addition, as bactofection has proven successful in treating melanoma and lung and colon carcinoma in mice, there is good reason to assume that microbots are also well suited to tumour treatment.

One of the attractive features of the microbots is that they permit targeted delivery, which should dramatically reduce the number of nanoparticles that need to be administered. Combining microbot-mediated nanoparticle delivery with recombinant protein expression in the bacteria could prove very useful in the targeted destruction of cancer cells. In particular, the fact that gene expression can be switched on in *L. monocytogenes*, specifically once they have entered the interior of host cells, opens attractive avenues[4]: for example, once they have entered the target cell, the microbots could deliver nanoparticles loaded with a relatively non-toxic 'prodrug', and the carrier bacteria could be chosen to express the protein that metabolizes the prodrug into its more potent, cytotoxic form. This would provide a highly specific lethal target for tumours, greatly limiting the side effects of conventional chemotherapy.

Advances in bactofection have so far been mostly incremental, but the Purdue team's approach of combining microbiology with nanotechnology could be a big step forward. As well as having scientific potential, the microbots also show what can be achieved when scientists from different disciplines get together and the Purdue microbiology/nanotechnology work should lead the way for other interdisciplinary research projects.

References

1. Akin, D. *et al. Nature Nanotech.* advance onine publication, 10 June 2007 (doi: 10.1038/nnano.2007.149).
2. Sizemore, D. R., Branstrom, A. A. & Sadoff, J. C. *Science* **270,** 299–302 (1995).
3. Darji, A. *et al. Cell* **91,** 765–775 (1997).
4. Dietrich, G. *et al. Nature Biotechnol.* **16,** 181–185 (1998).
5. Niethammer, A. G. *et al. Nature Med.* **8,** 1369–1375 (2002).
6. Souders, N. C., Verch, T. & Paterson, Y. *DNA Cell Biol.* **25,** 142–151 (2006).
7. Xiang, S., Fruehauf, J. & Li, C. J. *Nature Biotechnol.* **24,** 697–702 (2006).
8. Angelakopoulos, H. *et al. Infect. Immun.* **70,** 3592–3601 (2002).
9. Gentschev, I. *et al. Infect. Immun.* **63,** 4202–4205 (1995).

Bacteria-mediated delivery of nanoparticles and cargo into cells

DEMIR AKIN[1,2,3]*, JENNIFER STURGIS[2,4], KATHY RAGHEB[2,4], DEBBY SHERMAN[5], KRISTIN BURKHOLDER[6], J. PAUL. ROBINSON[2,3,4], ARUN K. BHUNIA[6], SULMA MOHAMMED[7] AND RASHID BASHIR[1,2,3,8]*

[1]Birck Nanotechnology Center, Purdue University, 1205 W State Street, West Lafayette, Indiana 47907, USA
[2]Bindley Biosciences Center, Purdue University, West Lafayette, Indiana 47907, USA
[3]Weldon School of Biomedical Engineering, Purdue University, 206 S Intramural Drive, West Lafayette, Indiana 47907, USA
[4]Department of Basic Medical Sciences, Purdue University, West Lafayette, Indiana 47907, USA
[5]Department of Biology, Purdue University, West Lafayette, Indiana 47907, USA
[6]Molecular Food Microbiology Laboratory, Department of Food Science, 745 Agriculture Mall Drive, West Lafayette, Indiana 47907, USA
[7]Department of Comparative Pathobiology, 725 Harrison Street, West Lafayette, Indiana 47907, USA
[8]School of Electrical and Computer Engineering, Purdue University, West Lafayette, Indiana 47907, USA
*e-mail: akin@purdue.edu; bashir@purdue.edu

Published online: 10 June 2007; doi:10.1038/nnano.2007.149

Nanoparticles and bacteria can be used, independently, to deliver genes and proteins into mammalian cells for monitoring or altering gene expression and protein production. Here, we show the simultaneous use of nanoparticles and bacteria to deliver DNA-based model drug molecules *in vivo* and *in vitro*. In our approach, cargo (in this case, a fluorescent or a bioluminescent gene) is loaded onto the nanoparticles, which are carried on the bacteria surface. When incubated with cells, the cargo-carrying bacteria ('microbots') were internalized by the cells, and the genes released from the nanoparticles were expressed in the cells. Mice injected with microbots also successfully expressed the genes as seen by the luminescence in different organs. This new approach may be used to deliver different types of cargo into live animals and a variety of cells in culture without the need for complicated genetic manipulations.

One of the most significant challenges facing the treatment of diseases is early intervention to deliver specific therapeutic cargo efficiently into cells to alter gene expression and subsequent protein production. Recent advances in nanotechnology have been used to deliver such cargoes into single cells through the use of nanoparticles for imaging[1–3], diagnostics[4,5] and therapeutics[6–8]. Although significant advances have been made, many difficulties remain in delivering the nanoparticles to the tumour sites, mainly because of the physical barriers encountered in solid tumours, such as malformed blood supplies, elevated interstitial pressure, and large transport distances in the tumour interstitium[9,10].

Bacteria have been used as a non-viral means to transfer plasmid DNA into mammalian cells through a process called 'bactofection' (reviewed in ref. 11). Several intracellular bacteria, including *Listeria monocytogenes*, which is responsible for food-borne infections in humans and animals[12], can penetrate mammalian cells that are normally non-phagocytic. These bacteria need specific surface molecules that interact with host-cell receptors for this invasion step[13–15] once inside the cells, the bacteria carriers are disrupted—by treatment with antibiotics—and the DNA is released. *L. monocytogenes*-based bactofection systems have shown efficient transfer of genetic material inside the cells[16,17]. Other earlier reports include use of attenuated (reduced infectivity) bacteria such as *Shigella*[18] and *Salmonella typhimurium*[19,20] for the delivery of DNA-based vaccines. Bacteria themselves have additional advantages as delivery systems. For example, attenuated strains of *Escherichia coli*, *S. typhimurium*, *Vibrio cholerae* and *L. monocytogenes* have been shown to be capable of multiplying selectively in tumours[21], and in the case of *Clostridium* and *Bifidobacterium* spp., they even inhibit tumour growth[20,22]. Some of the unique properties of attenuated Listeria strains make them an ideal non-viral gene delivery vehicle[23–25]. It should also be noted that antibiotics can control bacterial replication in the body or activate gene-based therapeutic molecules, as in the case with tetracycline-regulated control of gene expression[26].

Here, we report a novel technique for delivery of nanoparticles into cells, which takes advantage of the invasive properties of bacteria. The gene or cargo is not carried inside the bacteria, but rather remains on the surface conjugated to nanoparticles. Hence, our approach does not require bacterial disruption for delivery, or any genetic engineering of the bacteria for different cargo. Although more than one gene can be delivered by means of bactofection, many more copies of a target cargo can be carried with one bacterium using the method described here. We also show that nucleic acid-based model drugs (plasmid DNAs coding for green fluorescence protein (GFP), luciferase and secreted alkaline phosphatase (SEAP)) loaded on the nanoparticles can be released from the carriers and eventually find their way into the nucleus, with subsequent transcription and translation of their respective proteins, for both *in vitro* and

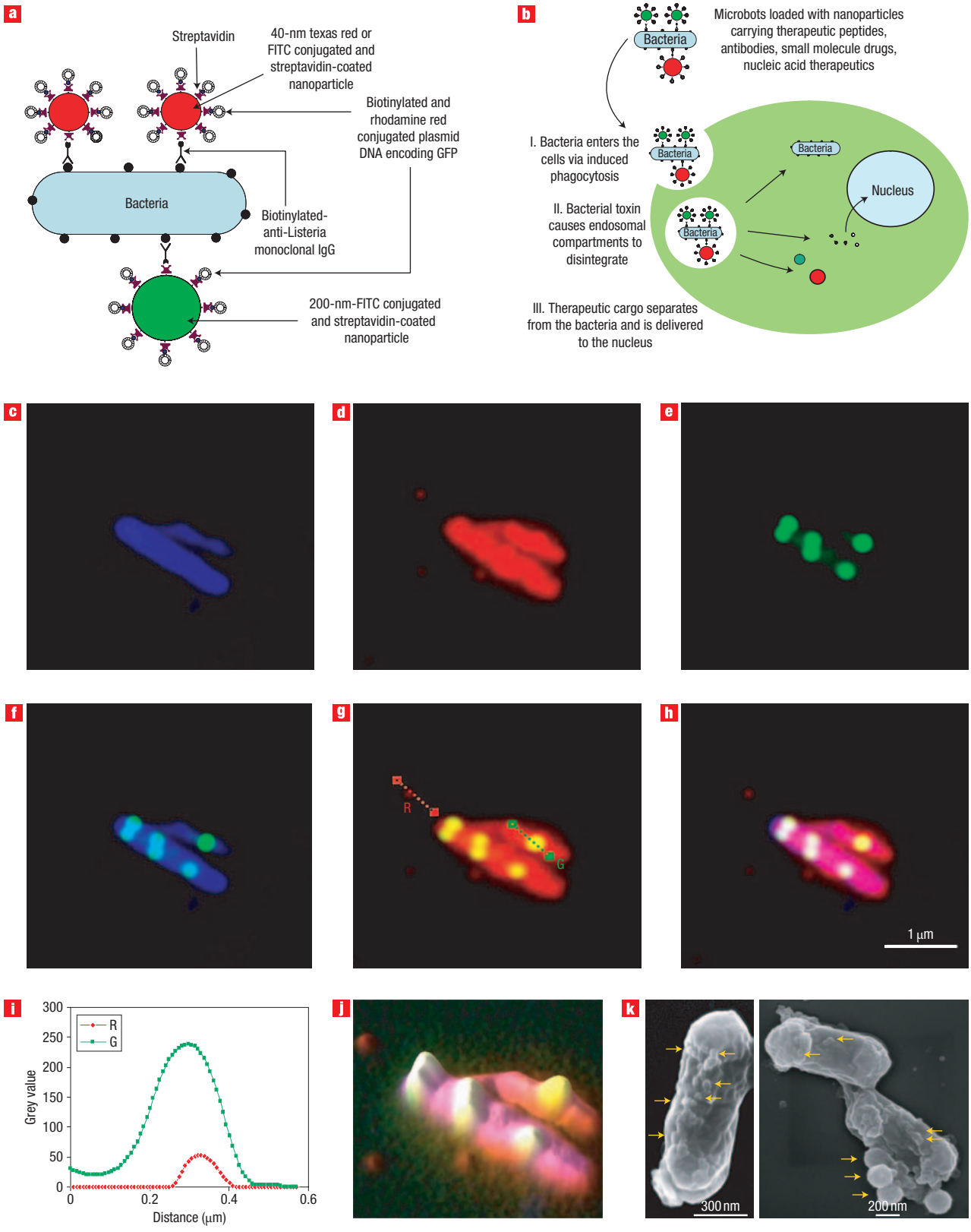

Figure 1 Bacteria-mediated delivery of nanoparticles and cargo. a, Docking of bacteria with functionalized multiple-sized nanoparticles through biotinylated antibodies and surface–antigen interactions (microbots). Streptavidin-coated nanoparticles can carry biotinylated cargo. **b**, Delivery of intervention agents using microbots. **c–k**, Assembled microbots with their cargos: bacteria (blue) (**c**), streptavidin-coated 40-nm fluorescent-red nanoparticles (**d**), neutravidin-coated 200-nm fluorescent-green nanoparticles (**e**). **f–h**, Overlays of images **c** and **e** (**f**), images **d** and **e** (**g**), and images **c–e** (**h**). **i**, Profiles of lines G and R from **g**. **j**, Simulated height image. **k**, SEM images of microbots (arrows show nanoparticles).

in vivo conditions. Such bacteria, which we call 'microbots', can potentially be used to carry proteins, small molecules and even synthetic objects like sensors and therapeutic moieties into different types of cells.

MICROBOTS DELIVER NANOPARTICLES AND DNA INTO CELLS

Our approach for preparing the microbots uses biotinylated monoclonal antibody C11E9[27,28] against a surface protein, N-acetylmuramidase[29], on *L. monocytogenes* bacteria to attach streptavidin-coated polystyrene nanoparticles onto the bacterial surface. Biotinylated GFP plasmid was then attached to the remaining streptavidin sites on the nanoparticles (Fig. 1a) (see Methods). This generalized approach can be used to attach particles of various sizes or different entities onto Listeria to be delivered into eukaryotic cells (Fig. 1b). We characterized the attachment of the particles on individual bacteria with fluorescence imaging (Fig. 1c–j) and scanning electron microscopy (SEM) (Fig. 1k). Fluorescence images of biotinylated antibody-covered Listeria incubated with streptavidin-coated 40 nm (red) and 200 nm (green) nanoparticles clearly show that the bacterium, which was stained blue, is co-localizing with the 40-nm Texas red-labelled nanoparticles and 200-nm FITC green-labelled nanoparticles (Fig. 1c–j), thus proving that the same bacteria can carry different size particles.

When fluorescently labelled bacteria were incubated with KB (human nasopharyngeal carcinoma) cells for up to 3 h at 37 °C, bacteria entered the cytosol of the cells and resulted in significant bacterial replication in the cells (see Supplementary Information, Fig. S1 and video). Incubation of the cells with the biotinylated anti-*L. monocytogenes* monoclonal antibody did not neutralize the infectivity of the microbots (see Supplementary Information, Table S1). We next attempted to deliver nanoparticles docked on the bacterial cell surface as described in the Methods. The 200-nm particles on their own were not internalized by the cells within the 3 h period, but rather were associated with the cell surface (Fig. 2a), as also verified by fluorescence imaging (Fig. 2b), whereas microbots successfully delivered the 200-nm particles inside the KB cells when incubated for 3 h (Fig. 2c). The nanoparticles were found in subcellular vesicle compartments and were also free in the cytosol. The yellow co-localization signal in the images (Fig. 2c) was due to red-labelled cellular membranes and green nanoparticles. Optical confocal slices proved that green fluorescent-labelled particles were indeed inside the cells and not on the cell surface (Fig. 2d) and approximately twenty 200-nm particles (on average) entered the cells when transported with the microbots (Fig. 2e).

Detailed flow cytometry analysis was also performed with partial cell lysis and secondary antibody immunostaining to prove and characterize the uptake of the nanoparticles mediated by the bacteria (Fig. 3a–d). As expected, the secondary anti-mouse antibody did not enter the cells to stain the monoclonal antibody C11E9 that was delivered into the cells by means of microbots (Fig. 3a) until the cells were lysed by a mild detergent treatment. The cells (lower left quadrants in Fig. 3b,c) were incubated separately with streptavidin-coated 200-nm particles (upper left quadrants in Fig. 3b,c), *L. monocytogenes* only (lower right quadrants in Fig. 3b,c) and microbots with streptavidin-coated 200-nm particles (upper right quadrants in Fig. 3b,c). After removal of the non-cell-associated material, the samples were either left untreated (Fig. 3b) or lysed with Triton-X100 (Fig. 3c). Subsequently, all samples were stained with a phycoerythrin (PE)-conjugated monoclonal antibody against mouse IgG and were subjected to flow cytometry analysis using dual channels for fluorescein isothiocyanate (FITC) (FL1) and PE (FL4). An analysis of the results of the PE readings (Fig. 3b,c) revealed that approximately 27% of the total PE signal (42%) was derived from intracellular sources, that is, from microbots (Fig. 3d). Approximately 15% of the total PE signal was either extracellular or cell membrane associated. Cells alone or KB cells with Listeria only samples did not have significant PE signals (Fig. 3d).

Microbots, docked with the model nucleic acid-based therapeutic GFP DNA, delivered the gene to the nucleus successfully, resulting in the expression of GFP as diffuse green fluorescence in the cytoplasm of KB cells (Fig. 4). Although the nanoparticles were intracellular at both 3 h (Fig. 4a) and 18 h (Fig. 4b) time points, the expression of GFP occurred at 18 h post-delivery (Fig. 4b,c). Dissociation of the nanoparticles from bacteria and the docked DNA from the nanoparticles may be facilitated by the low pH environment of the lysosomal compartments (Fig. 4d). Image analysis revealed a transfection efficiency of approximately $41.7 \pm 8.8\%$ (Fig. 4b,c; see also Supplementary Information, Fig. S5). The efficiency of bactofection has been reported to range from ~2 to 20% (ref. 16). In three of the four tested cell lines (Caco2, COS-1, HeLa, HepG2), the efficiency was extrapolated to be less than 10% for the same study. We believe that the higher transfection efficiency using our approach is due to both nanoparticle properties (their high surface-to-volume ratio, which allows more cargo to be loaded) and the number of nanoparticles that can be docked onto the bacterial surface.

CYTOTOXICITY OF MICROBOTS

We examined the cellular cytotoxic response to 40-nm and 200-nm streptavidin-coated fluorescent polystyrene nanoparticles and to bacteria with nanoparticles in four cell lines from human solid-organ tumours (MCF-7, KB, HeLa, HepG-2). All cells rapidly responded to the nanoparticles within 1 h with acute lactate dehydrogenase (LDH) release, but their response gradually decreased (see Supplementary Information, Fig. S7). When compared with detergent-damaged positive control samples, all cells incubated with 40-nm particles alone showed up to 60% cytotoxicity within 1 h. Over three days this response gradually decreased to 14% and cells were dividing, indicating that they were metabolically active. Neither Listeria nor microbots with nanoparticles caused a drastic cellular cytotoxic response; the response was less than for the particles alone. These samples had less than approximately 20% of the cytotoxicity of the detergent-lysed cells, except for the *L. monocytogenes* sample with the HepG-2 cell line, which had a cytotoxic response of ~40% (see Supplementary Information, Fig. S7b). Although the microbots had nanoparticles attached to them, the cells seemed to release more LDH for the nanoparticle-only samples. The 40-nm particles had higher cytotoxicity than the 200-nm particles because they can be taken up by the cells freely whereas the 200-nm particles are internalized only with the aid of microbots (Fig. 2). Invasion assays were also performed (see Supplementary Information, Fig. S7c) to evaluate the invasion efficiency of *L. monocytogenes*, *L. innocua* and the microbots for the four cell lines used in the study. The highest invasion was seen for the HepG-2 cells with *L. monocytogenes*.

GENE DELIVERY AND PROTEIN EXPRESSION IN MICE

Mice were injected intraperitoneally with microbots carrying the firefly luciferase gene on the 40-nm particle surface. Whole animal bioluminescence images (Fig. 5) showed that 3 days after infection, microbots successfully delivered the gene into the mice organs. The luciferase plasmid DNA was able to enter

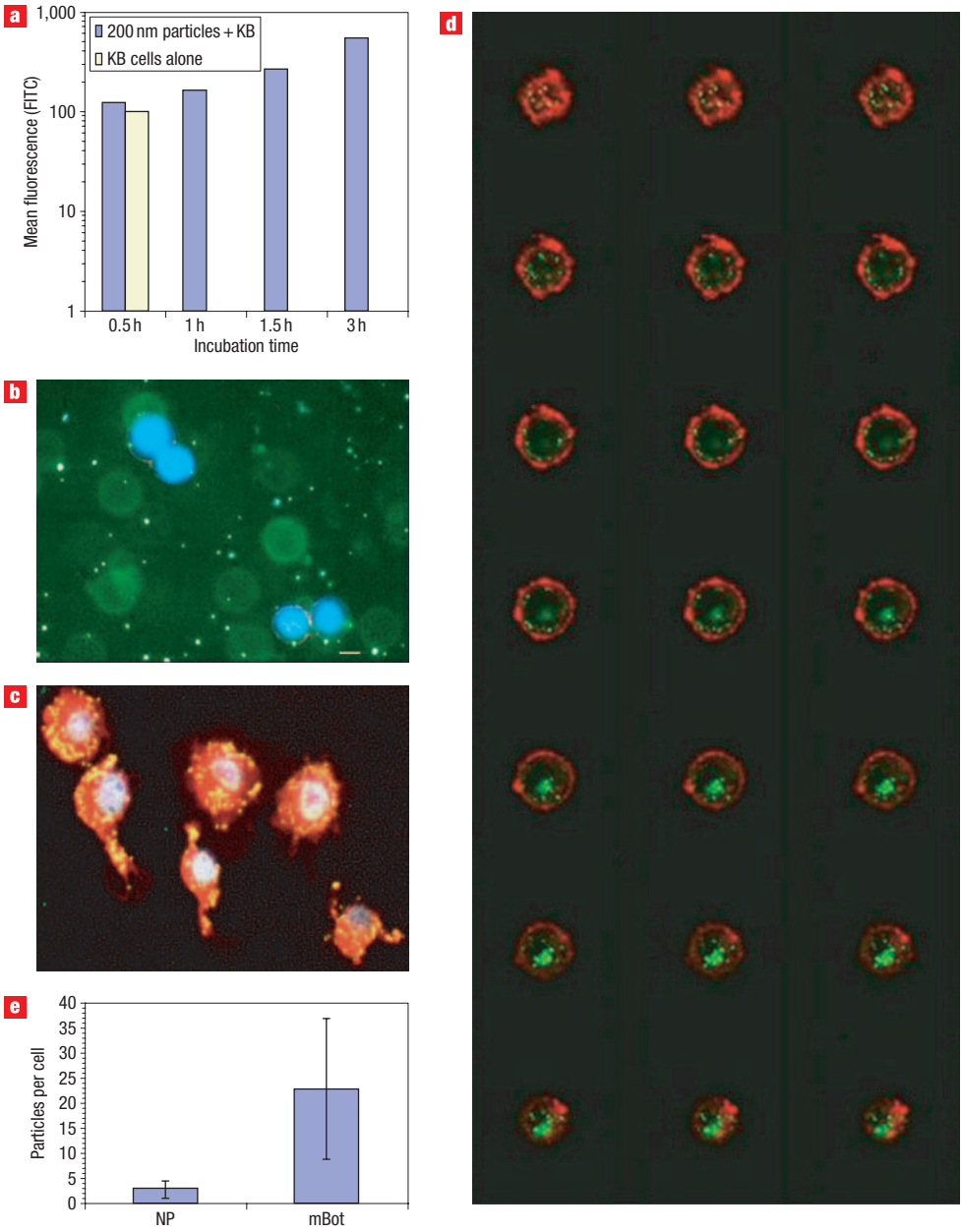

Figure 2 Internalization of microbots and their cargos. a, Time-dependent nonspecific association of 200-nm particles alone with KB cells. **b**,**c**, Fluorescence microscope images of cells incubated for 3 h with **b**, 200-nm particles alone (scale bar = 10 μm) and **c**, with microbots. **d**, Confocal microscope sections of a cell treated as in **c**, showing internalization. **e**, Average number of internalized nanoparticles per cell as calculated from panels **b–d** (NP, nanoparticle alone; mBot, with microbots). Cell membranes are red, nuclei are blue and nanoparticles are green in **b–d**. Yellow indicates internalization in **c**. Error bars represent standard deviations.

the nucleus and express the luciferase protein in the animals (Fig. 5a). There was no significant detectable endogenous luciferase activity in the animals injected with PBS as a control at 3 days post-injection (mean value 5 a.u., s.d. = 9.4, $n = 4$). Although all microbot-treated mice expressed the luciferase gene at a level of ~380-fold (3.81×10^4%) more than the controls, the level of expression was highly variable in each animal (mean value 1,908 a.u., s.d. = 1,451, $n = 3$), as indicated by the photon counts per square pixel area of the expression regions from Fig. 5a (see also Fig. 5b). We were also able to elucidate the location of the fluorescent nanoparticles using a fluorescence illumination and background elimination setup (described in the Supplementary Information, Methods), which enabled us to co-localize nanoparticle locations (Fig. 6a) and luciferase expression. The luciferase activity was seen throughout the internal organs, but seemed to localize in kidney, liver/pancreas, intestine, spleen, pericardium and lungs (in order of decreasing signal strength; Figs 5a and 6b–d). As is clearly evident in Fig. 6, the majority of the luciferase expression was localized in an area including the liver, pancreas, duodenum, spleen and kidneys. The kidneys had unambiguously high luciferase activity.

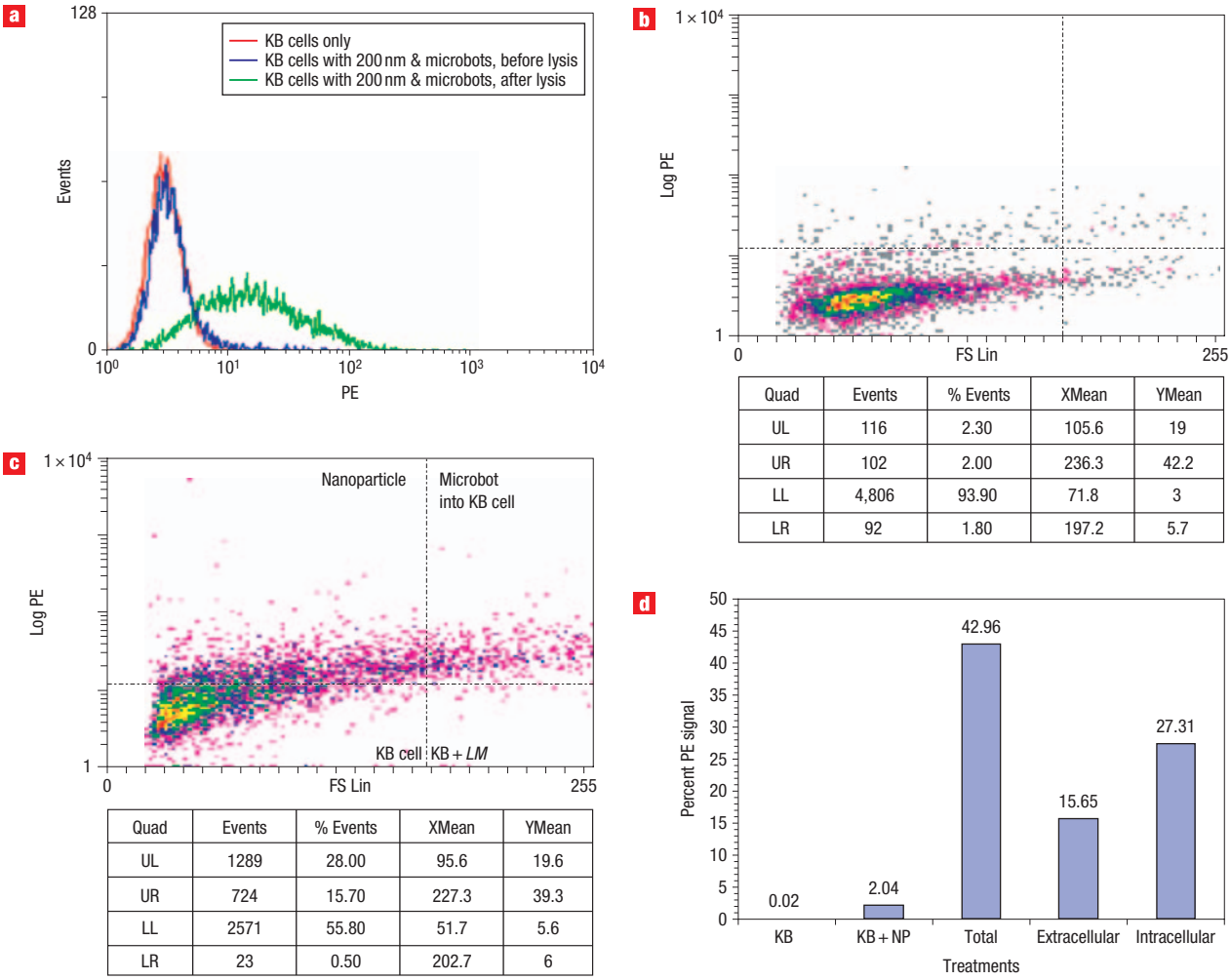

Quad	Events	% Events	XMean	YMean
UL	116	2.30	105.6	19
UR	102	2.00	236.3	42.2
LL	4,806	93.90	71.8	3
LR	92	1.80	197.2	5.7

Quad	Events	% Events	XMean	YMean
UL	1289	28.00	95.6	19.6
UR	724	15.70	227.3	39.3
LL	2571	55.80	51.7	5.6
LR	23	0.50	202.7	6

Figure 3 Flow-cytometric assessment of microbot uptake by cells. a, Evaluating the delivery of 200-nm particles into KB cells (red line) by flow cytometry. Treated cells were stained with phycoerythrin (PE)-labelled anti-mouse IgG antibodies before (blue line) and after (green line) cell lysis. Quantifying the internalization of **b**, nanoparticles alone and **c**, microbots. Quadrants in **b** and **c**: lower left (LL), KB cells; upper left (UL), 200-nm particles; lower right (LR), *L. monocytogenes* (*LM*) alone; upper right (UR), microbots with 200-nm particles; **d**, Evaluating the location of nanoparticles (NPs) with and without microbots. PE-labelled secondary antibody can access the interior of the cells only after cell lysis.

An alternative enzymatic method further verified the bioluminescence findings and quantified the microbot-mediated delivery and expression of the genes. Mice were injected with microbots carrying luciferase and SEAP gene cargoes and negative PBS-only controls. Three days later, select organs (liver, kidneys, spleen and intestines) were collected aseptically, enzymatically digested into homogenates and the expression of the reporter genes were quantified luminometrically (for luciferase) and chemiluminometrically (for SEAP). The luciferase assay had a signal half-life of 30 min, and, in preliminary assays, less than 5% signal intensity decay was observed within the reading time frame of the assays. In the luciferase and SEAP detection assay systems used, reporters yield linear assays with attomole sensitivities and no endogenous activity is associated with these reporters. Some intrinsic alkaline phosphatase activity can be found in various organs, but, being heat-labile, this enzyme is inactivated by treatment at 65 °C for 30 min, as was done here. Both luciferase (Fig. 6d) and SEAP (Fig. 6e) cargo molecules were delivered to the internal organs of live mice. Expressions of both reporter genes were highest in the intestinal tissue, which is also a natural target organ for *L. monocytogenes*. Kidney and liver samples from microbot-treated mice had noticeable amounts of luciferase and SEAP protein activity. Although not tested, the bioluminescence images showed noticeable levels of luciferase activity in the gall bladder, lungs and heart as well. Luciferase expression levels in the homogenates of the tested organs were highly variable, evident from the large standard deviations in the luciferase enzymatic activity (Fig. 6d). This could be due to variability in the efficiency of the SV40 promoter driving the luciferase gene in different tissues. The level of SEAP enzyme activity was more uniform in the tested organs (Fig. 6e). *L. monocytogenes*, injected via the intraperitoneal route can disseminate into the internal organs of mice, with a majority of the bacteria are found in the liver, spleen, kidneys, peripheral blood mononuclear cells and central nervous system[30,31]. In line with these previous reports, in our study, the bioluminescence due to luciferase activity was also localized in the liver, pancreas, duodenum, spleen and kidneys. Some activity in the intestine, lungs and heart was also seen at lower levels of intensity, a finding that has also been reported

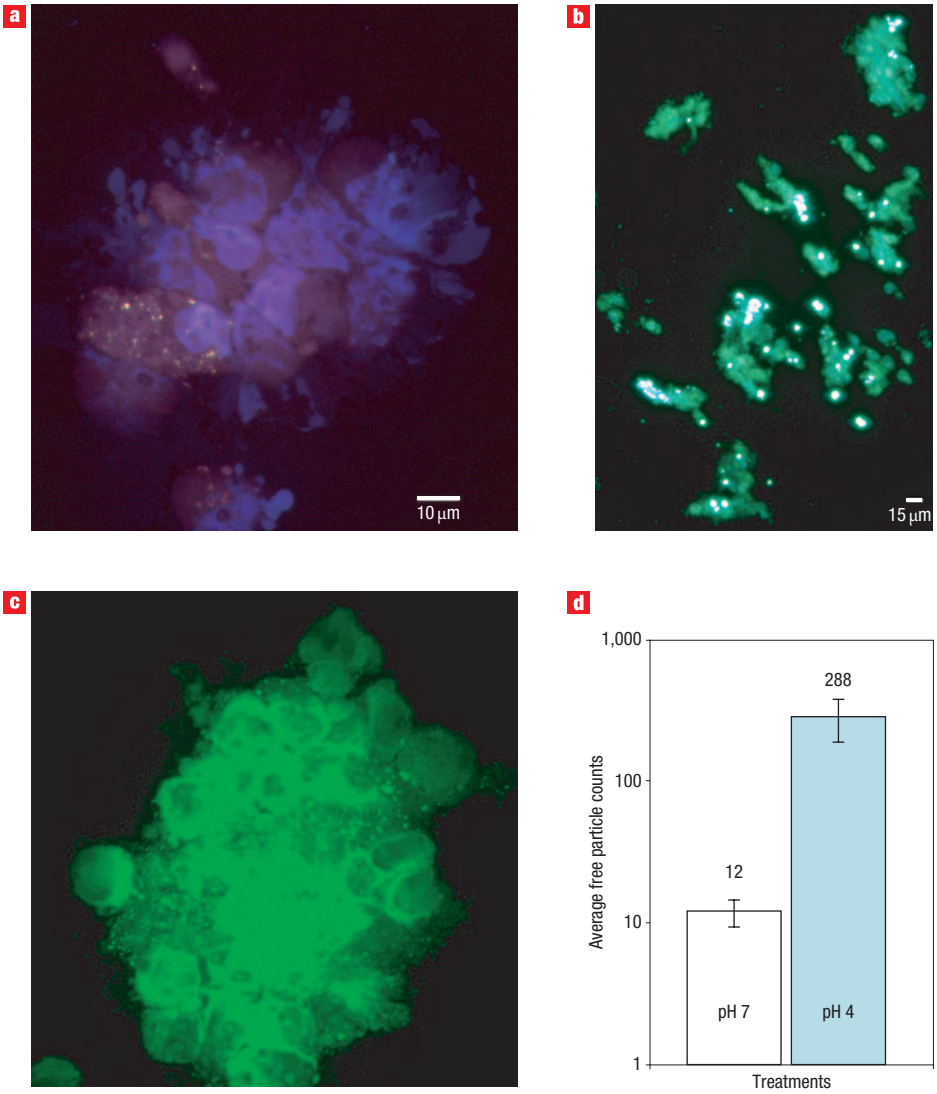

Figure 4 Intracellular delivery and expression of a model gene by microbots. a, Delivery of a plasmid DNA (coding for GFP) into KB cells using microbots at 3 h post-incubation. The cell membranes are red, nuclei are stained blue, and yellow indicates intracellular co-localization due to red (cells) and green (200-nm particles) signal overlap. **b**, A fluorescent micrograph (blue and green channels) of the sample in **a** at 18 h post-incubation. **c**, Expression of GFP from microbot-delivered DNA at a higher magnification (×1,000) at 18 h post-incubation. **d**, Disassociation of nanoparticles from the microbot surface at pH 4 and 7. Error bars represent standard deviations.

by others[32]. Signals seen around the lower thorax of the animals originate from the gall bladder, and this also has been well documented previously[32].

EFFICIENCY OF MICROBOT LOADING AND DELIVERY

From the confocal imaging studies, we found that each cell had approximately 22 200-nm particles (see Supplementary Information, Fig. S6). Because each microbot was carrying 1–3 particles, each human cell line used would therefore have at least 7–22 microbots. Previous immuno-electron microscopic analysis revealed a uniform distribution of C11E9 on the surface of *L. monocytogenes* cells, and the average number of C11E9-reactive antigens was approximately 190 per bacterium[25]; hence, it is reasonable to expect that a similar number of nanoparticles could be docked on each bacterial cell surface. The SEM images of the microbots (Fig. 1k) show that there are many 40-nm nanoparticles on the bacterial cell surface, supporting the previous findings that the cell surface receptors (N-acetylmuramidase) for antibody-C11E9 were uniformly distributed. This finding may also explain why microbots were fluorescing red in confocal and fluorescent microscopic images. The observed fewer numbers of 200-nm particles docked onto the bacterial cell surface may be due to steric hindrance, diffusion limitations or other physical barriers that preclude access or docking of 200-nm particles on the bacteria. Each 40-nm particle has a biotin-binding capacity of ~100, but for each 200-nm particle this value is 2×10^4 (from the certificate of analysis sheets of their manufacturer). Hence, each microbot is expected to carry biotinylated-DNA molecules in this range into target cells. The final spatial and temporal distribution of the microbots *in vivo* is determined by the invasion ability of *L. monocytogenes* for different tissue types and also by the filtration and sequestration of microbots or nanoparticles from the blood

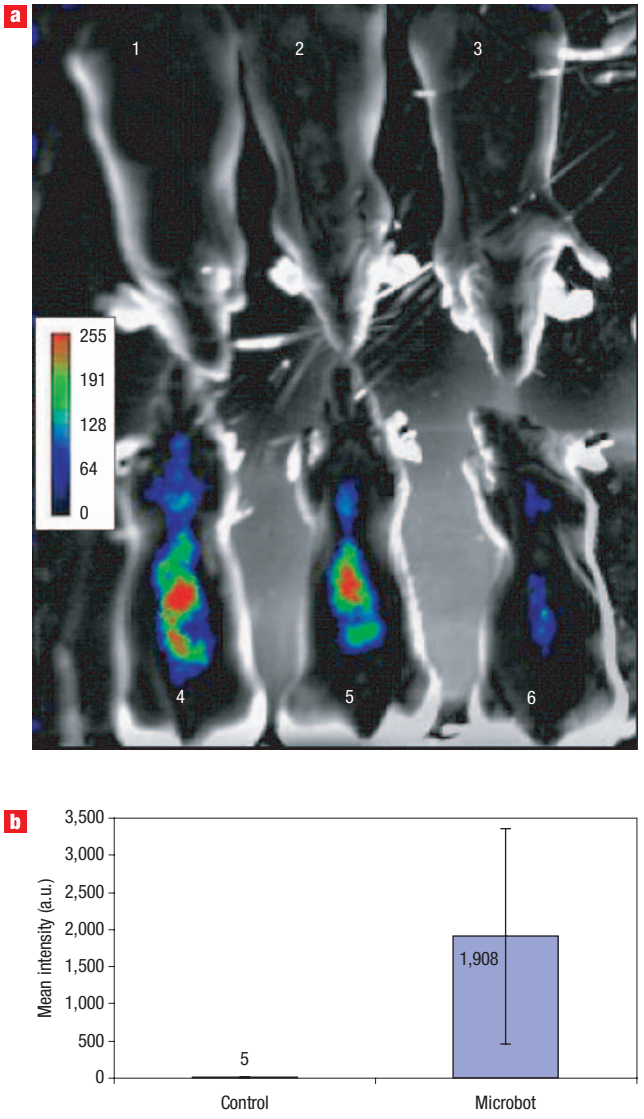

Figure 5 Microbot-mediated delivery and functional expression of luciferase gene in mice. a, In mice whole-animal bioluminescence images of mice with microbots carrying the firefly luciferase gene at three days post microbot treatment. Note the significant increase in photons collected from the microbot-treated animals (4–6) compared with the PBS-treated (sham-control) animals (1–3). The mice are in the ventro-dorsal position. **b**, Quantification of bioluminescence in sham-treated (white bar) and microbot-treated (blue bar) mice from **a**. On average, an ~380-fold increase in bioluminescence was observed in microbot-treated animals compared with PBS-treated mice ($n = 3$ animals per group, $P < 0.01$). Error bars represent standard deviations.

and lymphatic circulation system by different organs, in varying degrees.

DISCUSSION

In this study, we have demonstrated the bacteria-mediated delivery and visualization of different sized nanoparticles loaded with functional nucleic acid molecules into non-phagocytic mammalian cells of human solid organ tumours, and the successful expression of the cargo plasmid DNA (GFP) from the delivered nanoparticles. Liposomal or other encapsulated delivery methods suffer from the problem of entrapment in the subcellular vesicles and the biomolecule's inability to access the cytosol or other intended target sites such as the nucleus[33–36]. It is well known that *L. monocytogenes* can escape from the intracellular vesicles by means of the pore-forming activity of listeriolysin O. During this process the therapeutic molecules can diffuse into the cytoplasmic compartments. In a different approach reported earlier, *L. monocytogenes* was used to deliver DNA into the cytosol of mammalian cells by phage lysine mediated partial self-destruction of the carrier bacteria and by enhanced bacterial lysis due to the release of the intrinsically synthesized phage lysine[16].

Unlike these previously reported techniques, our approach is simple and versatile. Nanoparticles can be acquired commercially from various vendors, and have different surface functionalities, and different material and optical properties. Anchorage of the nanoparticles on the bacterial surface can easily be achieved using biotinylated antibodies, which serve as docking molecules through a streptavidin linkage. The 'nanovehicles' are linked to the bacteria by means of an antigen–antibody interaction, and the cargo and the bacteria can readily separate in the lower pH environment of the subcellular compartments, as made evident by the control experiments (Fig. 4d). Other factors, such as intracellular enzymatic processing or destabilization of antigen–antibody binding or a reduction in the biotin–streptavidin interactions can also be involved in the release mechanisms of the DNA, and all of these possibilities can potentially be used for endowing microbots with smart cargo release ability. Also, the use of intracellular bacteria in general and Listeria in particular for the delivery of nanoscale therapeutics has many advantages. Listeria bacteria have been shown to penetrate and colonize solid organ tumours[19,37] to which drugs circulating in the bloodstream have limited accessibility. Other nanoparticle-only based drug delivery approaches[38] still require the nanoparticles to be brought close to the tumour site, which is especially problematic in solid organ tumours and regions lacking vascularization.

In conclusion, microbots successfully delivered their cargos of nucleic acid-based model drugs, plasmid DNAs for firefly luciferase and SEAP enzymes into multiple organs of live mice, and the delivered genes also resulted in functional protein expression by three days post-treatment. As we have seen in the *in vitro* GFP expression assays, the delivered plasmid DNAs were able to escape from intracellular entrapment and were targeted to the nuclei of the cells, resulting in transcription and expression of the enzymes. Hence, this novel technology can be used to deliver these reporter molecules for whole-animal live imaging agents (luciferase) or for non-invasive *in vivo* reporter assays (SEAP). Our future studies will concentrate on the development of an attenuated Listeria strain, microbot-mediated delivery of artificial biohybrid nanostructures, delivery of larger size particles and functional proteins, and investigation of solid organ tumour penetration by microbots for applications in diagnostics and therapy at the single cell level and up to a few cells. Our bacteria-mediated nanoparticle and cargo delivery approach, which we term microbotics, promises excellent potential for nonviral gene delivery, and unique capabilities for biomedical nanorobotics and nanomedical therapy.

METHODS

PREPARATION OF MICROBOTS

Bacteria (10^8 colony forming units (c.f.u.) per ml, 1 ml) were incubated with a biotinylated monoclonal antibody C11E9[24–26] (1 μg ml^{-1}) at 22 °C for 30 min.

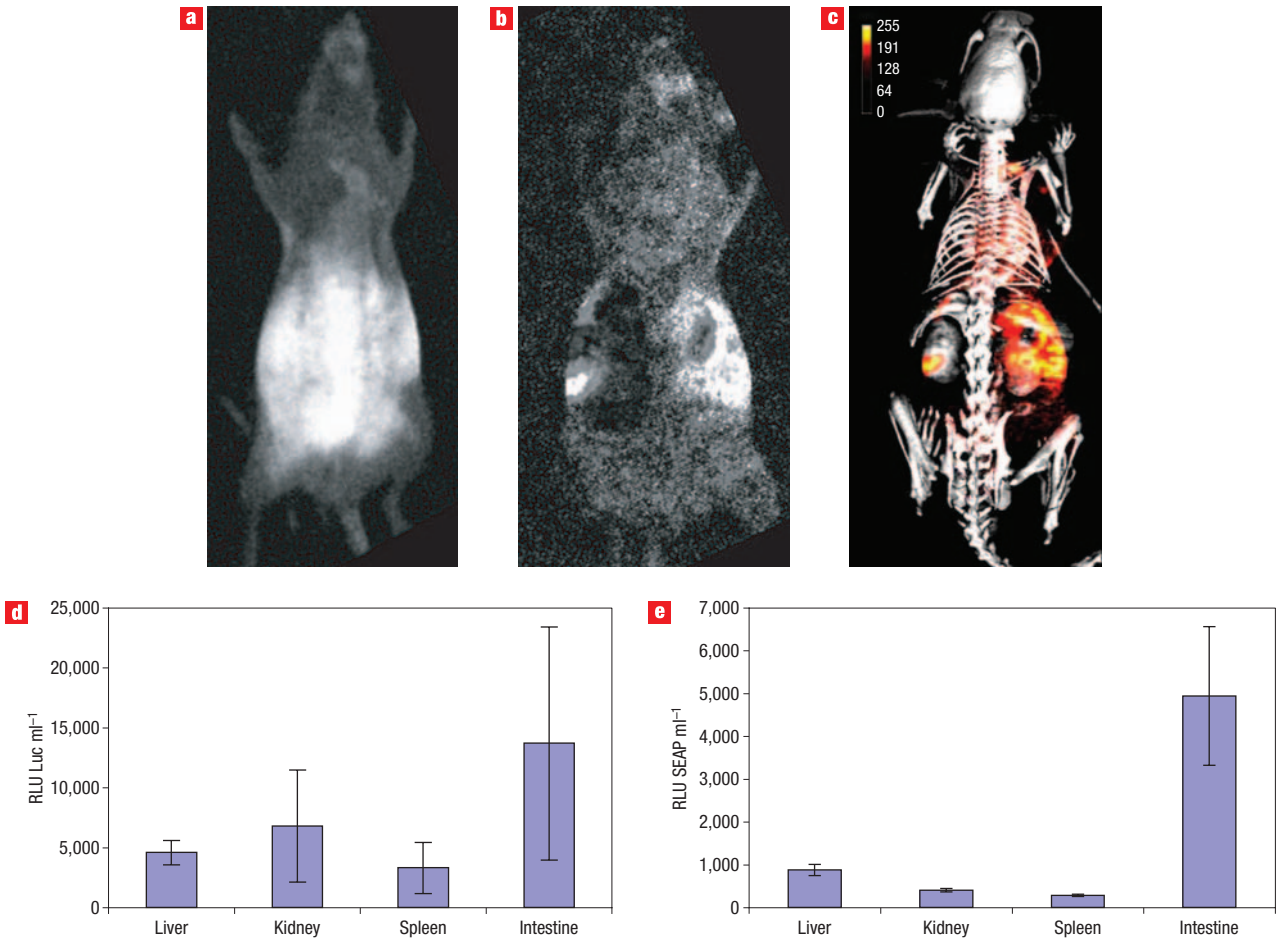

Figure 6 Characterization of *in vivo* protein expression. **a**, Live animal image of a mouse with microbots carrying the luciferase gene at three days post-injection. Locations of the nanoparticles were assessed by imaging (480 nm excitation, 523 nm band-pass emission-filter and 5 min exposure). **b**, A bioluminescence image of **a** with 35 min photon collection and integration. **c**, Anatomical localization of bioluminescence. A pseudo-coloured image of **b** was superimposed on a graphical anatomical image of a mouse to illustrate anatomical localizations of the signals. Mice are positioned ventro-dorsal in **a** and dorso-ventral in **b–c.** **d**, Enzymatic quantification of luciferase expression in organs of mice at three days post-injection. **e**, Enzymatic quantification of SEAP expression in organs of mice at three days post-injection (in relative light units, RLU). Error bars represent standard deviations.

After antibody attachment to the bacteria surface, two washes (see Supplementary Information) were performed to remove unreacted antibody. Streptavidin- or neutravidin-coated nanoparticles were then added (1×10^{10} ml^{-1}) and the mixture was incubated at room temperature for 15 min, at which time two low-speed washes were performed, and a centrifugal force of 3,000 *g* was applied for 5 min to preferentially spin down the bacteria, but not the nanoparticles. Microbots were diluted into PBS at 10^5 c.f.u. ml^{-1} and used immediately (or stored at 4 °C for no more than a week for SEM imaging studies). A biotinylated and rhodamine-labelled plasmid DNA vector encoding GFP under the control of a cytomegalovirus promoter (Gene Therapy Systems) was used as the model nucleic acid therapeutic molecule and was docked on the nanoparticle surfaces by streptavidin– or neutravidin–biotin interaction (see Supplementary Information, Methods, for details).

IMMUNOFLUORESCENCE ANALYSIS OF INTRACELLULAR AND EXTRACELLULAR MICROBOTS

After the initial infection process, cell monolayers were rinsed twice with PBS to remove unattached microbots and extra nanoparticles. Cells were trypsinized and recovered from the culture chambers, spun down at 300 *g* for 5 min and rinsed with Dulbecco's phosphate buffered saline (D-PBS) solution (Sigma) by performing a low-speed centrifugation as above. The cells were mounted on microscope slides and observed with a fluorescence microscope equipped with filters appropriate for FITC, Texas red and DAPI, and imaged using a cooled-colour CCD camera. Bacterial DNA was labelled with Hoechst-33342 stain for 15 min at room temperature. During some studies bacteria were also dual labelled with a lipophilic green-fluorescent cyanine-dye (DiO, Molecular Probes) and Hoechst stain.

FLOW CYTOMETRIC ASSESSMENT OF NANOPARTICLE UPTAKE

Tumour cells were grown in 24-well tissue culture plates to ~70% confluence and were rinsed with the fresh media. Either 40-nm or 200-nm nanoparticles were diluted in 10 μl of 1X Phosphate-Buffered Saline (PBS) to a final dilution of 0.01% (~10^9 particles) and were added to the wells of the tissue culture plate. The plates were returned back to the culture incubator and placed on a gently rotating stirrer for 0.5 h, 1 h, 2 h, 3 h and 3 days. To obtain cells in suspension, the cells were treated with 0.17% trypsin −0.02% EDTA (Sigma) at 37 °C for 1–3 min. Equal volumes of fresh medium were added to slow the digestion, and the cells were centrifuged at 300 *g* for 5 min. The supernatant was removed and the cells were washed once with wash buffer (PBS with 2% fetal bovine serum) as above. Finally, the cells were resuspended in the growth medium lacking serum and kept at 4 °C in an ice bath before being read in the flow cytometer. Each sample was assayed by flow cytometry (Epics XL, Coulter), and the data were analysed by both WinMDI and CellQuest software packages. To differentiate intracellular and extracellular microbots by fluorescence microscopy and flow cytometry, a dual-antibody staining procedure was used as described previously[39] and details are given in the Supplementary Information, Methods.

IN VIVO EXPRESSION STUDIES

Microbots were prepared as described above, except two different biotinylated plasmid DNAs coding for luciferase and SEAP were used instead of GFP[40]. The concentration of plasmid DNA per 100 µl of injection-ready microbot preparation was 5 µg DNA per 10^6 c.f.u. ml^{-1} of microbots, which were composed of 40-nm streptavidin-labelled Texas-red conjugated nanoparticles (10^{11} particles ml^{-1}) anchored on *L. monocytogenes* by means of monoclonal antibody C11E9. For analysis of *in vivo* delivery and expression, athymic (immunodeficient) nude mice ($Nu^{-}Nu^{-}$, all 5- to 6-week-old males, Harlan Sprague Dawley) were used throughout the studies as described in the Supplementary Information, Methods.

BIOLUMINESCENCE IMAGING

In vivo bioluminescence imaging was performed using a protocol detailed previously[20] using a Kodak Image Station and its acquisition and analysis software (Kodak). Additional image processing and quantifications were performed using ImageJ software (W. Rasband, National Institute of Health) as described in the Supplementary Information, Methods.

ENZYMATIC QUANTIFICATION ASSAYS FOR LUCIFERASE AND SEAP EXPRESSION

Organs (liver, kidneys, spleen and a small portion of the small intestine) from killed microbot-treated and untreated animals were collected aseptically into sterile plastic tubes and all subsequent sample processing was done on ice in these containers. All of the organs were homogenized separately in 200 µl reporter lysis buffer (Promega) on ice, centrifuged at 12,000 *g* for 1 min, and the supernatants were divided into two equal-sized aliquots and immediately used in the luciferase or SEAP assays, on the same day. For quantification of expression of luciferase, a kit-based assay in 96-well format (Promega) was used according to the instructions of the manufacturer of the kit.

ADDITIONAL METHODS

Additional details on the cell culture, invasion assays, nanoparticles, cytotoxicity assay, flow cytometry, confocal and bioluminescence imaging and analysis and enzymatic quantification of firefly luciferase and SEAP are available in the Supplementary Information.

Received 8 February 2007; accepted 2 May 2007; published 10 June 2007.

References

1. Chan, W. C. & Nie, S. Quantum dot bioconjugates for ultrasensitive nonisotopic detection. *Science* **281,** 2016–2018 (1998).
2. Gao, X. *et al.* In vivo molecular and cellular imaging with quantum dots. *Curr. Opin. Biotech.* **16,** 63–72 (2005).
3. Lin, Z., Su, X., Mu, Y. & Jin, Q. Methods for labeling quantum dots to biomolecules. *J. Nanosci. Nanotech.* **4,** 641–645 (2004).
4. Voura, E. B., Jaiswal, J. K., Mattoussi, H. & Simon, S. M. Tracking metastatic tumor cell extravasation with quantum dot nanocrystals and fluorescence emission-scanning microscopy. *Nature Med.* **10,** 993–998 (2004).
5. Ballou, B., Ernst, L. A. & Waggoner, A. S. Fluorescence imaging of tumors in vivo. *Curr. Med. Chem.* **12,** 795–805 (2005).
6. West, J. L. & Halas, N. J. Engineered nanomaterials for biophotonics applications: improving sensing, imaging, and therapeutics. *Annu. Rev. Biomed. Eng.* **5,** 285–292 (2003).
7. Seppenwoolde, J. H. *et al.* Internal radiation therapy of liver tumors: qualitative and quantitative magnetic resonance imaging of the biodistribution of holmium-loaded microspheres in animal models. *Magn. Reson. Med.* **53,** 76–84 (2005).
8. Hattori, Y. & Maitani, Y. Enhanced in vitro DNA transfection efficiency by novel folate-linked nanoparticles in human prostate cancer and oral cancer. *J. Control. Release* **97,** 173–183 (2004).
9. Jain, R. K. Haemodynamic and transport barriers to the treatment of solid tumors. *Int. J. Radiat. Biol.* **60,** 85–100 (1991).
10. Maeda, H., Wu, J., Sawa, T., Matsumura, Y. & Hori, K. Tumor vascular permeability and the EPR effect in macromolecular therapeutics: a review. *J. Control. Rel.* **65,** 271–284 (2000).
11. Vassaux, G., Nitcheu, J., Jezzard, S. & Lemoine, N. R. Bacterial gene therapy strategies. *J. Pathol.* **208,** 290–298 (2006).
12. Vazquez-Boland, J. A. *et al.* Listeria pathogenesis and molecular virulence determinants. *Clin. Microbiol. Rev.* **14,** 584–640 (2001).
13. Finlay, B. B. & Cossart, P. Exploitation of mammalian host cell functions by bacterial pathogens. *Science* **276,** 718–725 (1997).
14. Vazquez-Boland, J. A., Dominguez-Bernal, G., Gonzalez-Zorn, B., Kreft, J. & Goebel, W. Pathogenicity islands and virulence evolution in *Listeria*. *Microbes Infect.* **3,** 571–584 (2001).
15. Hamon, M. L., Bierne, H. & Cossart, P. *Listeria monocytogenes*: a multifaceted model. *Nature Rev. Microbiol.* **4,** 423–434 (2006).
16. Pilgrim, S. *et al.* Bactofection of mammalian cells by *Listeria monocytogenes*: improvement and mechanism of DNA delivery. *Gene Ther.* **10,** 2036–2045 (2003).
17. Dietrich, G. *et al.* Delivery of antigen encoding plasmid DNA into the cytosol of macrophages by attenuated suicide *Listeria monocytogenes*. *Nature Biotechnol.* **16,** 862–866 (1998).
18. Sizemore, D. R., Branstrom, A. A. & Sadoff, J. C. Attenuated Shigella as a DNA delivery vehicle for DNA-mediated immunization. *Science* **270,** 299–302 (1995).
19. Darji, A. *et al.* Oral somatic transgene vaccination using attenuated *S. typhimurium*. *Cell* **91,** 765–775 (1997).
20. Paglia, P., Medina, E., Arioli, I., Guzman, C. A. & Colombo, M. P. Gene transfer in dendritic cells, induced by oral DNA vaccination with *Salmonella typhimurium*, results in protective immunity against a murine fibrosarcoma. *Blood* **92,** 3172–3176 (1998).
21. Yu, Y. A. *et al.* Visualization of tumors and metastases in live animals with bacteria and vaccinia virus encoding light-emitting proteins. *Nature Biotechnol.* **22,** 313–320 (2004).
22. Bermudes, D., Zheng, L. M. & King, I. C. Live bacteria as anticancer agents and tumor-selective protein delivery vectors. *Curr. Opin. Drug Discov. Devel.* **5,** 194–199 (2002).
23. Loeffler, D. I., Schoen, C. U., Goebel, W. & Pilgrim, S. Comparison of different live vaccine strategies in vivo for delivery of protein antigen or antigen-encoding DNA and mRNA by virulence-attenuated *Listeria monocytogenes*. *Infect. Immun.* **74,** 3946–3957 (2006).
24. Souders, N. C., Verch, T. & Paterson, Y. In vivo bactofection: Listeria can function as a DNA-cancer vaccine. *DNA & Cell Biol.* **25,** 142–151 (2006).
25. Souders, N. C., Sewell, D. A., Pan, Z. K., Hussain, S. F., Rodriguez, A., Wallecha, A. & Paterson, Y. Listeria-based vaccines can overcome tolerance by expanding low avidity CD8+ T cells capable of eradicating a solid tumor in a transgenic mouse model of cancer. *Cancer Immun.* **7,** 2–12 (2007).
26. Weber, W. & Fussenegger, M. Inducible gene expression in mammalian cells and mice. *Methods Mol. Biol.* **267,** 451–466 (2004).
27. Bhunia, A. K *et al.* Development and characterization of a monoclonal antibody specific for *Listeria monocytogenes* and *Listeria innocua*. *Infect. Immun.* **59,** 3176–3184 (1991).
28. Geng, T. *et al.* Expression of cellular antigens of *Listeria monocytogenes* that react with monoclonal antibodies C11E9 and EM-7G1 under acid-, salt- or temperature-induced stress environments. *J. Appl. Microbiol.* **95,** 762–772 (2003).
29. Geng, T., Hahm, B. K. & Bhunia, A. K. Selective enrichment media affect the antibody-based detection of stress-exposed *Listeria monocytogenes* due to differential expression of antibody-reactive antigens identified by protein sequencing. *J. Food Prot.* **69,** 1879–1886 (2006).
30. Drevets, D.A. Dissemination of *Listeria monocytogenes* by infected phagocytes. *Infect. Immun.* **67,** 3512–3517 (1999).
31. Bron, P. A., Monk, I. R., Corr, S. C., Hill, C. & Gahan, C. G. Novel luciferase reporter system for in vitro and organ-specific monitoring of differential gene expression in *Listeria monocytogenes*. *Appl. Environ. Microbiol.* **72,** 2876–2884 (2006).
32. Hardy, J., Margolis, J. J. & Contag, C. H. Induced biliary excretion of *Listeria monocytogenes*. *Infect Immun.* **74,** 1819–1827 (2006).
33. Miller, A. D. The problem with cationic liposome/micelle-based non-viral vector systems for gene therapy. *Curr. Med. Chem.* **10,** 1195–2110 (2003).
34. El-Aneed, A. An overview of current delivery systems in cancer gene therapy. *J. Control. Rel.* **94,** 1–14 (2004).
35. Lechardeur, D. & Lukacs, G. L. Intracellular barriers to non-viral gene transfer. *Curr. Gene Ther.* **2,** 183–194 (2002).
36. Cheong, I. *et al.* A bacterial protein enhances the release and efficacy of liposomal cancer drugs. *Science* **314,** 1308–1311 (2006).
37. Michl, P. and Gress, T. M. Bacteria and bacterial toxins as therapeutic agents for solid tumors. *Curr. Cancer Drug Targets.* **4,** 689–702 (2004).
38. Braun, L., Nato, F., Payrastre, B., Mazie, J. C. & Cossart, P. The 213-amino-acid leucine-rich repeat region of the *Listeria monocytogenes* InlB protein is sufficient for entry into mammalian cells, stimulation of PI 3-kinase and membrane ruffling. *Mol. Microbiol.* **34,** 10–23 (1999).
39. Tang, P., Foubister, V., Pucciarelli, G. & Finlay, B. B. Methods to study bacterial invasion. *J. Microbiol. Methods* **18,** 227–240 (1993).
40. Zreiqat, H., Sungaran, R., Howlett, C. R. & Markovic, B. Quantitative aspects of an in situ hybridization procedure for detecting mRNAs in cells using 96-well microplates. *Mol. Biotechnol.* **10,** 107–113 (1998).

Acknowledgements

The authors would like to thank C. Koons, Drug Discovery Shared Resource of Purdue Cancer Center, for her help with the *in vivo* studies, S. Leavesly for his inputs in the initial bioluminescence imaging studies, C. Buck for assisting in the use of the facilities at Bindley Biosciences Center, and the Weldon School of Biomedical Engineering for funding the work. D.A. was supported by funds from NIH NIBIB.

Correspondence and requests for materials should be addressed to D.A. and R.B.

Supplementary information accompanies this paper on www.nature.com/naturenanotechnology.

Author contributions

D.A. and R.B. designed the experiments. D.A. performed and was involved in all aspects of the experiments; J.S. performed confocal and fluorescence imaging; K.R. and J.P.R. performed the flow cytometery; and D.S. performed the SEM imaging. D.A., K.B. and A.B. designed and performed the cytotoxicity studies. S.M. assisted in *in vivo* studies. D.A. and R.B. co-wrote the paper.

Competing financial interests

The authors declare no competing financial interests.

SUPPLEMENTARY INFORMATION

Supplementary Methods

Cell Culture. The following cancer cell lines derived from human solid organ tumors were used in the study: HeLa (ovarian cancer), HT-29 (colon adenosarcoma), MCF-7 (breast cancer), KB (oral carcinoma), Caco-2 (colon carcinoma), HepG-2 (hepatocarcinoma). These cells were adherent phenotype and were originally obtained from ATCC (ATCC, Manassas, VA). They were propagated in DMEM supplemented with 10% fetal bovine serum and were maintained in a 5% CO_2 atmosphere at 37°C. The cells were regularly split every other day or when they reach ~80% confluency. *Listeria innocua* and *L. monocytogenes V7* (LmV7) was maintained on bovine heart infusion (BHI) agar plates and propagated in Luria Bertani (LB) medium at 37°C. Mid logarithmic phase bacteria were used for the infection experiments. Throughout the infection or cell culture growth or maintenance no antibiotics were used except when we attempted to assess the location of the NPs after the infection process or during the invasion assays.

Nanoparticles. Streptavidin or neutravidin-immobilized green (200nm, 40nm) or red (40nm) fluorescent polystyrene particles (1 and 0.5% solids content, respectively) were purchased from a commercial source (FluoSpheres, Invitrogen, Carlsbad, CA) and were used as supplied by the manufacturer throughout the study. Prior to use, particles were vortexed vigorously for 1-3 min and their concentrations were adjusted to $1x10^{10}$ particles per ml. The original concentration of the 200nm particles was $2x10^{12}$ particles/ml and that of 40nm ones were $1.1x10^{14}$ (40nm green) and $2.3x10^{14}$ (40nm red) particles/ml.

Preparation of *Microbots*. Bacteria *(L. monocytogenes*) from mid-logarithmic growth phase were rinsed with phosphate buffered saline (PBS) twice by spinning the bacteria down in a table-

top centrifuge at 10000xg for 5min, removing the supernatant, and re-suspending them in PBS. Briefly, the plasmid DNA (1ng/ml) in sterile distilled water was added to the PBS solution containing *Microbots* with nanoparticles and the mixture was incubated for 15min. At the end of the incubation period, the plasmid DNA-*Microbot* complexes were centrifuged at 800xg for 5 min to spin down the complexes and to separate free plasmid DNA. Then, the fully assembled *Microbots* with their model cargo were rinsed twice with PBS and resuspended in the same solution. These samples were used within one hour to carry out the intracellular cargo delivery experiments.

Characterization of Monoclonal Antibody C11E9's Effect on the Invasion of Caco-2 Cells by *Listeria*. *L. monocytogenes*, *L. innocua* and a recombinant *L. innocua* expressing *hly* gene[1] products were grown to mid-logarithmic phase in BHI medium. The bacteria were rinsed with PBS and were incubated for 1h with 0-1 μg/ml of biotinylated-anti-*Listeria* monoclonal antibody C11E9. Then, the mixture was used to inoculate Caco-2 cells in multi-well tissue culture plates (~70-80% confluent, ~$1x10^5$cells/ml). Assay was performed with a multiplicity of infection (*m.o.i.*) of about 10:1. Caco-2 cells were exposed to bacteria for 1h. Cells were washed with PBS thrice to remove excess bacteria, and monolayers were treated with 20 μg/ml gentamicin for 1h to kill any extracellular bacteria. At the end of the antibiotic treatment, the cells were lysed with 0.01% Triton-X 100 and intracellular bacteria were enumerated by plating on BHI agar plates. Triplicate counts were obtained and were statistically analyzed.

Flow Cytometric Assessment of Nanoparticle Uptake. Briefly, KB cells (2×10^6 cells) were grown overnight in six-well tissue culture plates and the cells were infected with *L. monocytogenes* at an *m.o.i.* of 100:1 for 1-3h, washed twice with D-PBS, and incubated with gentamicin (100μg/ml)-containing medium for 1h. The monolayers were washed again to remove non-adherent bacteria and nanoparticles. Since extracellular *Listeria* were stained blue

by Hoechst stain and they also contained a biotinylated-mouse monoclonal anti-*Listeria* antibody (C11E9-IgG) on the bacterial cell surface, a rabbit anti-mouse phycoerythrin (PE)-labeled (dilution, 1:100 in PBS, Invitrogen, Carlsbad, CA) antibody was used to stain *Microbots* before and after a cell permeabilization procedure. Cell monolayers were then permeabilized with 0.2% Triton X-100 for 2min to allow staining of both intracellular and extracellular *Listeria* (total *Listeria*). Coverslips were mounted with a mounting solution and observed with a Nikon Eclipse-600 fluorescence microscope and also submitted for flow cytometry analysis. The number of intracellular *Listeria* organisms was obtained by subtracting the mean fluorescence of the PE channel of extracellular *Listeria* (before Triton lysis) from the number of total *Listeria* organisms (after Triton lysis).

Cytotoxicity Assays. The effect of nanoparticles and also the bacteria on cell viability was assessed by measuring lactate dehydrogenase (LDH) release as previously described[2]. Briefly, cells (~$1x10^6$) were plated at 7500 cells/well in 96-well plates in 100µl of fresh medium. After 24h the medium was replaced with 200µl of fresh OPTI-MEM (Invitrogen, Carlsbad, CA)) serum-free medium, containing the samples. Cells were then incubated with the samples consisting of either nanoparticles, nanoparticles docked on the bacteria or bacteria alone at 37^oC in 5% CO_2 for various times ranging from 0.5h, 1h, 2h, 3h and 3 days. The cells were infected with an *m.o.i.* of approximately 10:1 (bacteria:cells) wherever Listeria was used during the cytotoxicity assays. An index of cell death was obtained by measuring LDH release in cell supernatants using a cytotoxicity detection kit (Roche Applied Science, Indianapolis, IN) according to the protocol supplied by the manufacturer. At the each end point time, both negative controls (spontaneous release) and positive maximum releasable LDH treatments were also included. Negative controls received PBS as inoculums instead of the samples described above.

Mock treated cells were lysed by 10min incubation in 0.01% final concentration of Triton-X 100 in PBS at the end of the incubation periods to obtain the maximum amount of releasable LDH. Each assay from each time point and each cell line and also each treatment sample were run as triplicate samples. Following formula was used to calculate the cytotoxic responses to the treatments which were expressed as percent LDH release.

Percent Cytotoxic Response=100*(Treatment-Spontaneous Release) / (Triton Lysed-Spontaneous Release)

Antibiotic Protection Method for Determination of Cellular Invasion. For the bacterial invasion assay, bacterial cultures were harvested by centrifugation at 10,000xg for 10 min, and were washed three times in 0.2 M phosphate buffered saline (PBS), pH 7.4. The optical densities of bacterial cultures were adjusted to 0.3 using a spectrophotometer (Beckman Coulter) at 595 nm. Eukaryotic cells ($1x10^5$cells/ml) in 48-well tissue culture plates were washed 1 time with DMEM containing 10% fetal bovine serum, and 5µl bacterial cultures were added to the media in cell culture wells, for an approximate *m.o.i.* of 10:1 bacteria to cancer cells. Plates were incubated for 3h at 37°C in 5% CO_2. Following the incubation, cell culture medium was removed from the monolayers by gentle aspiration using an 8-channel multi-pipettor. All of the subsequent wash and treatment steps were done using sterile reagents. Monolayers were washed three times by adding 500µl of PBS via a multi-channel pipettor, followed by gentle aspiration of the wash buffer. After the primary wash steps, 500µl of tissue culture medium containing 20µg/ml gentamicin was added to each well, and the plates were incubated at 37°C for 1h with 5% CO_2 to kill extracellular and surface adherent bacteria. The monolayers were again washed thrice with PBS. Finally, 500µl of 0.05% Triton X-100 was added to each well and the plates

were incubated for 10min at 37°C in order to disrupt the epithelial cell monolayers and liberate intracellular bacteria. The bacteria were enumerated by plating on bovine heart infusion (BHI) agar in triplicate replicas from serial 10-fold dilutions in PBS. Invasion rate was defined as (intracellular CFU) / (Inoculum CFU) x 100.

Confocal, Fluorescence and Scanning Electron Microscopy. Cells on Labtek^{TM} slides were observed under a confocal microscope (Radiance 2100 Multiphoton Microscope, Bio-Rad, Inc) at Purdue University Cytometry Laboratories. Scanning electron microscopy (SEM) was performed in NanoSEM system (Fei Company, Hilsboro, OR) at 5kV at 100,000 X magnification. The bacterial samples on a 1x1cm silicon chip were fixed with formaldehyde and were coated with a thin metal before the SEM imaging was performed. For the confocal and fluorescence microscopy, no fixation steps were used.

Image Analysis. Images from each color channel were acquired using a triple filter set as high resolution TIFF images. Image manipulations (contrast, brightness, gamma) and analysis were performed with ImageJ software[3]. Colocalization signal analysis and spectral unmixing were performed by using ImageJ plugins (RGB colocalization, spectral unmixing, respectively). *Microbot*-mediated transfection efficiency was defined as the ratio of cells not expressing GFP and cells expressing GFP.

***In-vivo* Expression Studies.** DNA that was used for the expression of SEAP was obtained as a purified plasmid DNA from a commercial source (pGeneGrip-biotin-SEAP, Gene Therapy Systems, SanDiego, CA) as biotinylated DNA (25 μg/ml). Plasmid DNA for the expression of firefly (*Photinus pyralis*) luciferase was derived from a plasmid vector (pGL3-luc, Promega, Madison, WI) which was biotinylated using a kit (Sigma, St. Louis, MO) and a previously

published protocol[4]. Expression of the luciferase gene was from the SV40 promoter and that of the SEAP was from CMV promoter. For analysis of *in-vivo* delivery and expression, athymic (immunodeficient) nude mice ($Nu^{-}Nu^{-}$, all 5 to 6 –week old males, Harlan Sprague Dawley Inc., Indianapolis, IN) were used throughout the studies. The animals were housed under sterile conditions in microisolator cages and allowed to acclimate for 5 days before the injections. They were given *ad libitum* access to food and water. All animal housing and surgical procedures were performed in accordance with the guidelines of Purdue University Animal Care and Use Committee and were performed at the Drug Development Shared Resources of the Purdue Cancer Center at Purdue University.

Bioluminescence Imaging. We carried out preliminary trials where we injected GFP expressing *L.monocytogenes* subcutaneously to determine if GFP could be used as a possible reporter, as we did in our *in-vitro* studies, that will be delivered into nude mice as expression ready plasmid DNA by Microbots for live animal imaging. However, autofluorescence of the skin and other underlying tissues precluded discrimination of weak signals in our measurement systems. Due to the lack of endogenous sources of luciferase in normal animals, firefly luciferase is an attractive reporter for *in-vivo* imaging and was used in the *in-vivo* animal studies described in the main text of the paper.

Plasmid DNA alone or *Microbots* carrying the plasmid DNA for firefly luciferase were injected intra-peritonealy (*i.p.*) in 150µl amounts per mice. As negative controls same volume of sterile PBS was injected. Five mice per treatment group were used in the imaging studies. Prior to bioluminescence imaging mice were anesthetized with a premixed cocktail of a dosage of 10 mg/kg body weight xylazine and 90 mg/kg body weight ketamine via. *i.p.* route and sodium salt of D-luciferin (Anaspec, San Jose, CA) at a concentration of 220µg per gram of body weight in

sterile 5% dextrose was injected by *i.p.* route. Ten minutes after the injections of luciferin, the mice were placed on the surface of the imaging device, a dim-light image was taken, and a series of increasing duration images were collected without any illumination initially to determine the optimal exposure times. Later on, the emitted light was acquired for 35min and integrated. This luminescence image was median filtered by using a 7x7 to 50x50 pixel progressively increasing integration matrix and overlaid on dim-light images to determine location of the emitted light. Luminescence signals were normalized to background signals from the untreated mice as setting the later to threshold cut-off value. Signal intensity was converted to grey scale values as the sum of all detected photon counts from a whole mouse after subtraction of background luminescence per mouse measured from the sham-treated (PBS) animals. From these images pseudocolor images representing the spatial distribution of photon counts produced by active luciferase within the tissues of the animal were generated.

Enzymatic Quantification Assays for Luciferase and SEAP Expressions. Prior to SEAP assays, the aliquots dedicated for this assays were incubated at 65°C for 30min in an incubator to inactivate intrinsic alkaline phosphatase (secreted alkaline phosphatase is heat stable under these conditions per manufacturer's specifications). The quantification of SEAP was done using a chemiluminescent SEAP assay kit (Great EscAPe SEAP Reporter System 3, Clontech Laboratories, Mountain View, CA) according to the instructions provided by its manufacturer.

A fluorescence-luminescence multi-detection microplate reader and its data acquisition software (BioTek Instruments, Inc. Winooski, VT) were used for the measurement of luminescence (luciferase) and chemilumiscence (SEAP) signals. Data was acquired for 15seconds with autosensitivity setting and all of the readings were summed together. For the quantification of both luciferase and SEAP expression levels, assays were run in triplicate on plates with the

following control wells: PBS only (background), *Microbot*-treated samples with DNA-docked on the *Microbots*, and DNA only injected samples, PBS-injected samples (sham treatment) and recombinant luciferase which had a specific activity of $\geq 2.0 \times 10^{10}$ light units/mg of luciferase protein (Quantilum recombinant luciferase, Promega) as positive control. Relative light units (RLU) values were recorded, and percent of expression was calculated as percent of expression = (1 – (mean RLU in *Microbot*-treated wells per average RLU of PBS)).

Supplementary Results

Flow Cytometric Characterization of Intracellular Delivery by Microbots. The flow data were analyzed by first comparing the forward-scatter versus side-scatter density plots for cells only and cells and nanoparticles or cells and *Microbots*. As the cells internalize nanoparticles and *Microbots,* side scattering is expected to increase. Since the non-adherent nanoparticles and *Microbots* are removed, the KB cells should have increasing forward scattering signal due to intense fluorescence of the particles.

Cytotoxic response to nanoparticles and *Microbots*. We examined the cellular cytotoxic response to 40nm and 200nm streptavidin-coated fluorescent polystyrene nanoparticles and to bacteria with nanoparticles in different cell lines. It was separately shown that 40nm particles were internalized by KB cells easily without the *Microbots* even in 1.5h (**Supplementary Fig. 2**), whereas the 200nm particles were not internalized on their own in KB cells and other cells lines even up to 3h incubation (**Fig. 2a**, **b**, and **Supplementary Figs. 3, 4**). The four human solid organ tumor cells (MCF-7, KB, HeLa, HepG-2) were incubated with the 40nm and 200nm nanoparticles individually (**Supplementary Fig. 7a**), or *L. monocytogenes*, *L. innocua*, or the *Microbots* with the docked nanoparticles (**Supplementary Fig. 7b)** for 0.5 h, 1 h, 2 h, 3 h, and 3 days in the growth medium. At the end point times, their LDH release, an early indication of membrane damage, was quantified from the cell supernatants by using a commercial cytotoxicity assay kit. The cells rapidly responded to the nanoparticles within 1 h via acute LDH release but their response gradually decreased (**Supplementary Fig. S7**). There was up to 60% cytotoxic response to 40nm particles alone within 1h in all cells as compared to the detergent damaged positive control samples and by three days this response gradually decreased to 14% and cells

were dividing, indicating that they were metabolically active. Neither *Listeria* spp. nor *Microbots* with nanoparticles caused a drastic cellular cytotoxic response; the response was less than the particles alone. These samples had approximately less than 20% cytotoxicity of the detergent-lysed cells, except for the *L. monocytogenes* sample with HepG-2 cell line which had a cytotoxic response of ~40% (**Supplementary Fig. 7b**). Although the *Microbots* had nanoparticles attached to them, the cells seem to release more LDH with the nanoparticle only samples. The cytotoxic response to the 40nm particle is higher than that of the 200nm particles since 40nm particle can be taken up by the cells freely, whereas 200nm particles are not internalized well without the aid of the *Microbots* (**Fig. 2**). Invasion assays were also performed (**Supplementary Fig. 7c**) to evaluate the invasion efficiency of *L. monocytogenes*, *L. innocua*, and the *Microbots* to the four cell lines used in the study, with the highest invasion seen for the HepG-2 cells with *L. monocytogenes*.

Microbot Injection and Antibiotic Administration In Animals. Up to the second day, any mice from any treatment group didn't show overt signs of Listerial infection; however, on day 3, the Microbot-injected group showed rapidly developing infection due to *L. monocytogenes*. During the preliminary studies where a dose escalation study (from 10^4-10^7 CFU/ml of *L. monocytogenes*) was performed to find out maximum tolerated dose for *L. monocytogenes*, the mice started showing signs of infection on the third and fourth days post injection when the *Microbots* were introduced subcutaneously (*s.c.*); however, the animals started showing signs of infection at the end of the second day when the route of administrations was *i.p.* As soon as the infection was noticed at the end of the second day, we administered antibiotics (sulfamethoxazole:trimethoprim, 30 mg/kg, *i.p.*) to all of the mice. During the subsequent studies we started the antibiotic administration at the beginning of day 2 to all animals regardless of if

signs of infection were present or not. For final *in-vivo* expression studies, *i.p.* route was used due to its higher systemic access potential than the *s.c.* route which may decrease the systemic access of *Microbots* in a time dependent manner.

We examined if we could locate the nanoparticles in internal organs and co-localize the expression of luciferase with the locations of the nanoparticles (**Fig. 6**). The nanoparticles (40nm) that we docked on the *Listeria* cell surface were red fluorescent and using an 480nm excitation light source and a 523nm band-pass filter built into the imaging device, we took 5 min exposure images of the mice injected with the *Microbots* and sham controls (PBS). Light emissions below 523nm were blocked by the band pass filter, hence majority of the auto-fluorescence signals were eliminated (**Fig. 6a**). The same animals were also imaged for bioluminescence in dark without the filters and the excitation light sources turned on for 35 min photon collection and 7x7 to 50x50 median pixel integration filters (**Fig. 6b**) and these images were pseudo-colored and overlaid on an image showing the anatomical structures of a mouse (this later CT scan image was obtained from http://www.ornl.gov/sci/eere/PDFs/FactSheet_BioIP_.pdf).

Enzymatic activities derived from the expression of *Microbot* delivered plasmid DNAs for the corresponding genes in each organ was expressed as background corrected relative light units (RLU) meaning that sham-treated control measurements were subtracted from the *Microbot* treated organ measurements. The arbitrary light units generated from the luminescence and chemiluminescence signals were converted to RLUs by using standard curves generated from recombinant sources of luciferase and alkaline phosphatase per instructions of the used kits and they were reported in **Fig. 7**.

Supplementary Discussions

In our cell invasion assays, both *L. monocytogenes* and *Microbots* were virulent and had invasive abilities as much as 1000-fold larger than the non-pathogenic species, *L. innocua*. Docking of the nanoparticles on the bacterial cell surface seemed to increase the uptake of the bacteria for the cells and the reasons for this behavior remain to be investigated. Wild type *L. monocytogenes* is pathogenic for the cells as expected; however, future use of this technology will investigate the use of intracellular replication-deficient listerial vaccine strains since these are shown to be cleared rapidly from the circulation in *in-vivo* studies with both immuno-competent and immuno-compromised mice[5] and humans[6]. Although the nanoparticles alone, particularly the 40nm nanoparticles, caused a significant cytotoxicity initially by 1h, the *Microbots* with same particles did not produce the similar response. The reason for this may have been due to the heavy aggregation behavior of the internalized nanoparticles alone which may have caused physical damage to the intracellular environment. Once the nanoparticles are released from the bacterial cell surface they may also aggregate and cause damage but this effect would be much less than the introduction of the 40nm nanoparticles alone. The level of the cellular toxicity of the 200nm nanoparticles either alone or immobilized on the *Microbot* surface was very similar, except in HepG-2 cells which are derived from hepatocarcinomas, there was an elevated response to 200nm particles alone. Even though relatively few larger nanoparticles are delivered into the cells, they have an increased surface area and hence more room for immobilization of additional cargo.

The cells used in our study are non-phagocytic and derived from epithelial origin[7] hence they don't naturally have the ability to phagocytize large particles as normally seen by the specialized phagocytic cells such as polymorphonuclear leukocytes, dendritic cells, and macrophages.

It can be speculated that after the *i.p*. injections, bacteria accessed the blood stream and reached the primary filtration organs such as kidneys, liver and spleen. It is likely that some of these *Microbots* were phagocytosed and gained access to various organs or entered the lymphatic circulation and trapped at the lymph nodes and or lymphatic tissues. It is also likely that some dissociated or *Microbot* preparation contaminant nanoparticles trapped in the lungs given their small size of only 40nm. The majority of the luciferase expression seen as bioluminescence was seen in kidneys, liver, spleen and intestines (**Fig. 5a**, **Fig. 6, Fig. 7a**). This finding was also confirmed by the enzymatic luciferase and SEAP expression assays performed on the organ homogenates of *Microbot*-injected and un-injected animals (**Fig. 7a** for luciferase and **Fig. 7b** for SEAP). Both reporter enzymes were highly expressed in intestines, yet, kidneys and liver had relatively higher luciferase activity than that of SEAP. To better quantify targeting of different organs by *Microbots*, we have used organ homogenates and performed enzymatic quantification for luciferase and SEAP enzyme activity which clearly showed biodistribution of the reporter enzyme activities. To better understand the full range of tissue distribution of *Microbots*, nanoparticles and expression of plasmid DNA and also promoter effects further detailed studies are needed.

Supplementary Tables

Table 1

Bacteria	% Invasion	
	0 µg/ml C11E9	**1 µg/ml C11E9**
L. monocytogenes	0.372 ± 0.017	0.389 ± 0.022
L. innocua WT	0.016 ± 0.001	0.018 ± 0.002
L. innocua hly+[a]	0.067 ± 0.008	0.064 ± 0.009

[a] Recombinant *L. innocua* carrying hemolysin gene from *L. monocytogenes*

Table 1. Influence of monoclonal antibody C11E9 on the invasion ability of Listeria to mammalian cells. In a standard infectivity assay using Caco-2 cells indicated Listeria with or without biotinylated monoclonal antibody C11E9 attached to the bacterial cell surface were allowed to infect the cells (*m.o.i*=10:1). After the invasion, extracellular bacteria were rinsed away and the cells were treated with gentamicin. Intracellular Listeria resulting from the invasion was enumerated by standard colony counting after the cells were lysed by a detergent treatment. No significant change was observed in the ability of the bacteria to infect the cells between the antibody-treated or untreated groups.

SUPPLEMENTARY FIGURES

Figure Legends

Supplementary Figure 1 (Video): A videomicroscopic recording of *L. monocytogenes* infection of KB cells. a, Bacterial infection is causing protrusions of bacteria-filled vesicles where bacteria can be seen to move rapidly, **b**, *L. monocytogenes* is moving in the cytoplasm of the infected KB cells.

Supplementary Figure 2: Internalization of 40nm nanoparticle in KB cells without microbots. a, Optical confocal slice images of a cell with 40nm streptavidin-coated polystyrene particles. **b**, 3D projections of a cell with 40nm streptavidin-coated polystyrene nanoparticles which have been internalized.

Supplementary Figure 3: Video microscopic analysis of nanoparticle delivery by *Microbots*. a, Videos of 3D projection of a cell with 200nm green streptavidin-coated polystyrene particles (with GFP plasmid) internalized with the aid of the *Microbots*. **b**, Video of 3D projection of a cell with 200 nm green streptavidin-coated polystyrene particles located mainly on the surface. Without *Microbots*, the nanoparticles are not internalized.

Supplementary Figure 4: Lack of internalization of 200nm green-fluorescent streptavidin-coated polystyrene nanoparticles by cancer cells from solid organ tumors. The cells (MCF-7, HT-29, KB, HeLa, HepG-2) were incubated with the nanoparticles for 3h in the growth

medium and their fluorescent signal emissions were quantified using a flow cytometer after rinsing three times in ice-cold PBS. It can be clearly observed that no significant uptake of the nanoparticles is taking place and any increase in fluorescence intensity is attributable to surface attachment of nanoparticles.

Supplementary Figure 5: Calculation of *in-vitro* efficiency of DNA delivery and expression. Efficiency of the expression was calculated from florescent microscopic images as a percentage of cells expressing GFP after the delivery of plasmid DNA. A sample image is shown above. Transfection efficiency was approximately 41.69±8.58 %.

Supplementary Figure 6: Efficiency of *in-vitro* DNA delivery. KB cells were treated with approximately equal concentrations of 200nm green-fluorescent particles alone (**a**) or docked on Listeria (**b**). Microbots were also prepared by docking only 40nm red fluorescent particles on a GFP expressing *L.monocytogenes* and delivered into the cells (**c**) and colocalization of the red nanoparticles with GFP fluorescence which produce yellow color, is clearly visible and internalization of these microbots are evident in the confocal optical z-slices. On average, there are 23 ± 14 200nm nanoparticles per cell in microbot-treated cells and 3 ±1.7 in nanoparticle only treated cells per confocal slice (**d**, slice thickness was 200nm). Each 200nm particle has a biotin binding capacity of $2x10^4$ per NP. Hence about $4.6±2.8x10^5$ DNA molecules are introduced into each infected cell. Nanoparticles per cell are given as per section of confocal slice.

Supplementary Figure 7: Analysis of invasion and toxic response of the cells treated with *L.monocytogenes* and *Microbots* carrying 40nm and 200nm polystyrene particles. a, Various cells (MCF-7, KB, HeLa, HepG-2) were incubated with 40nm or 200nm particles alone, separately. **b**, Various cells in **a** were incubated with *L. monocytogenes* or Microbots (*Microbots-mB*) for 0.5h, 1h, 2h, 3h, and 3 days in the growth medium. At the end point times, their LDH release was quantified by using a commercial cytotoxicity assay kit. Spontaneously releasable LDH was subtracted from both experimental and maximum releasable amounts and the experimental release was expressed as percentage of the total releasable LDH. Legend: Lm: *L. monocytogenes*, mB: *Microbot*, Tx-100: Triton-X 100 treated (lysed) cells. % Cytotoxicity = (Experimental – Spontaneous Release)/(Triton Released – Spontaneous Release) x 100. **c**, Invasion ability of *Listeria* and *Microbots* for cancer cells from solid organ tumors (MCF-7, HT29, KB, HepG-2). *L. monocytogenes* (Lm), *L. innocua* (Li) and *L. monocytogenes*-based *Microbots* (mB) docked with 40nm and 200nm streptavidin-coated polystyrene particles were incubated with the cancer cells for 3h. Then the extracellular bacteria were killed by gentamicin treatment and the intracellular bacteria released by gentle detergent treatment were enumerated by colony counting on BHI agar plates. Invasion ability was compared to the colony counts from original inoculum that was used to prepare the samples.

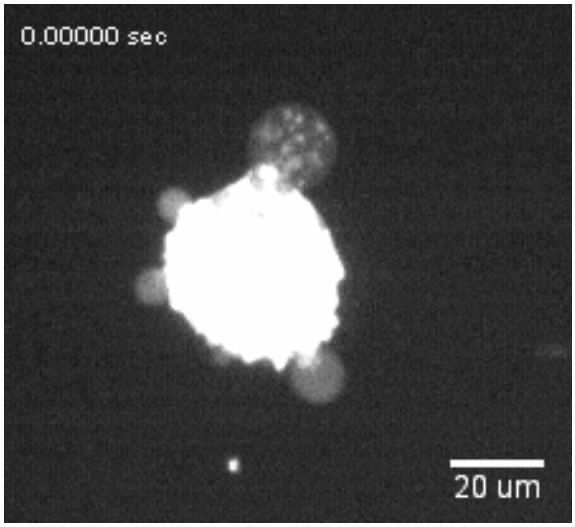

(a)

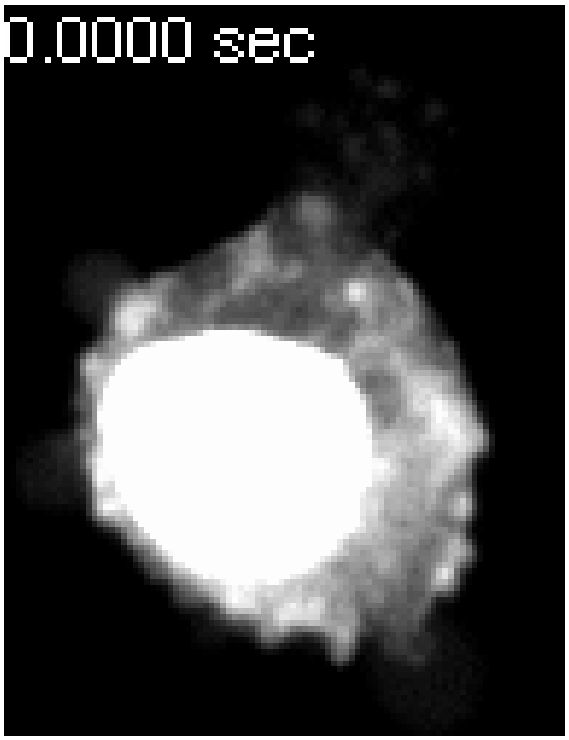

(b)

Supplementary Figure 1 (Video).

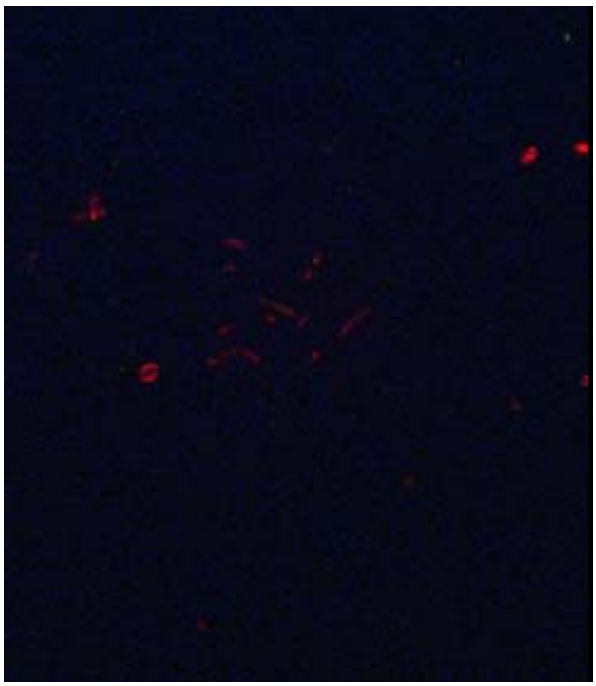

(a)

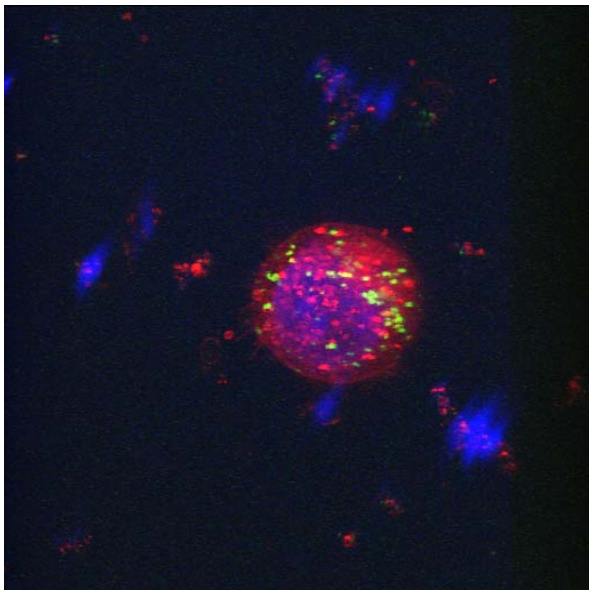

(b)

Supplementary Figure 2

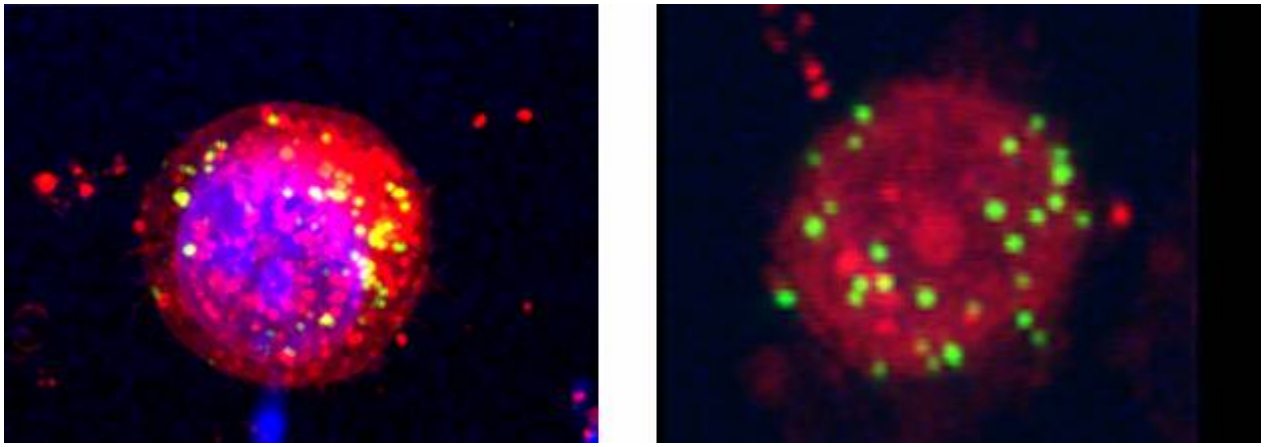

(a) **(b)**

Supplementary Figure 3

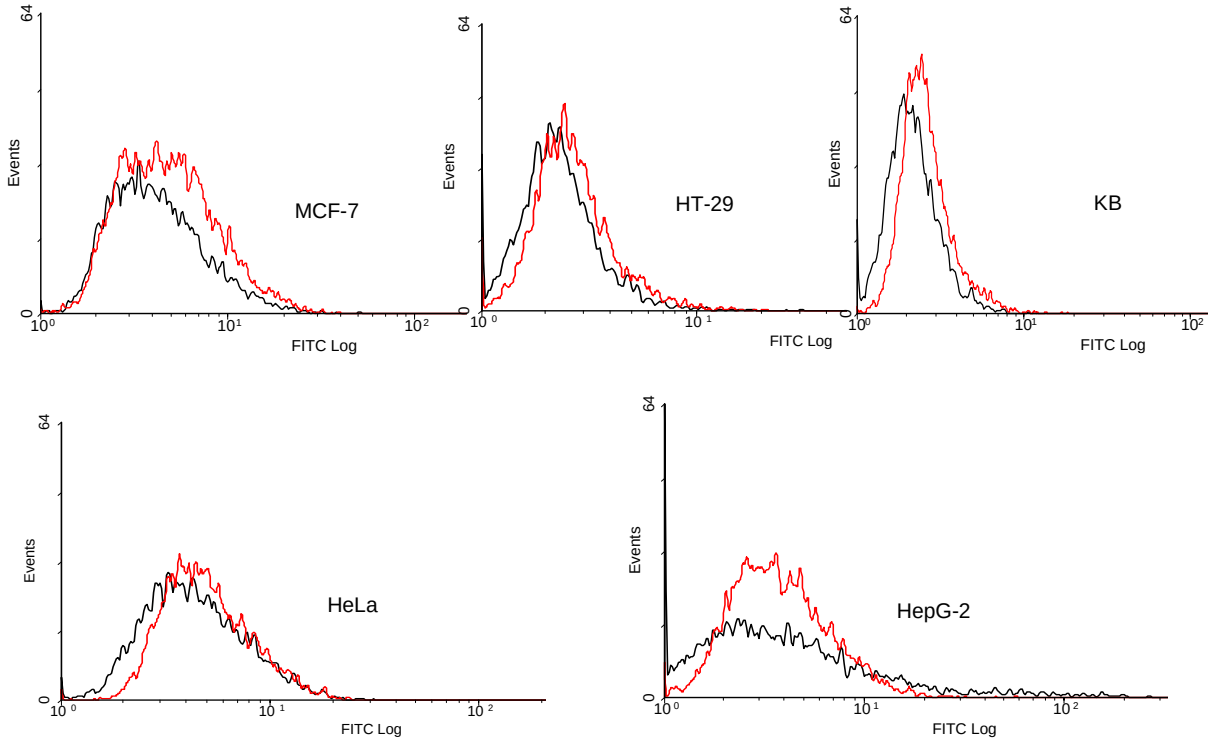

Supplementary Figure 4

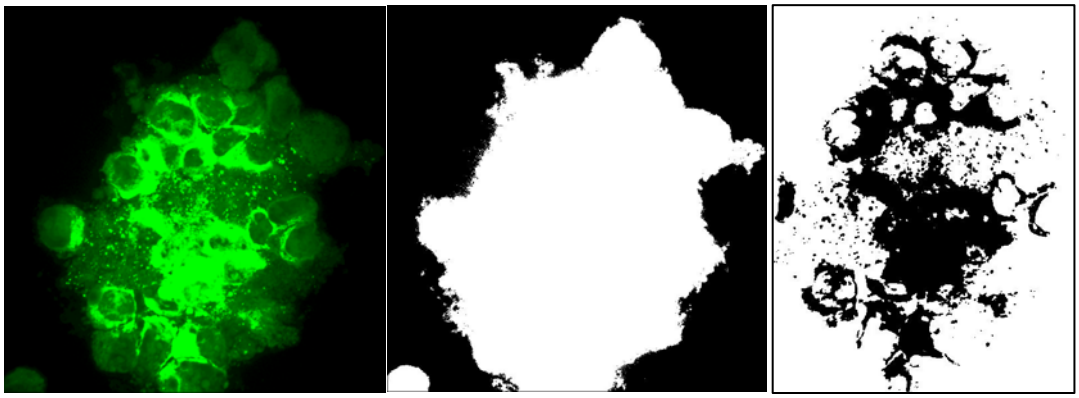

Supplementary Figure 5

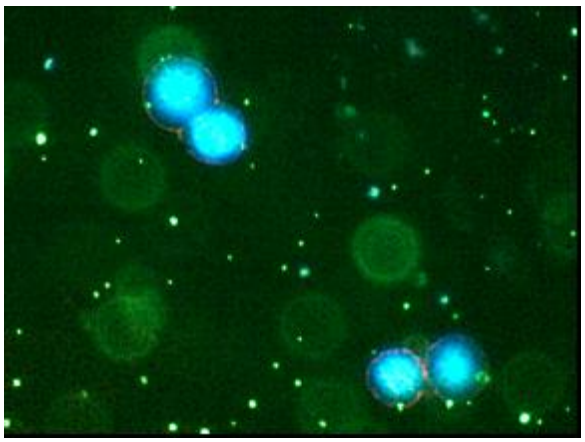

(a)

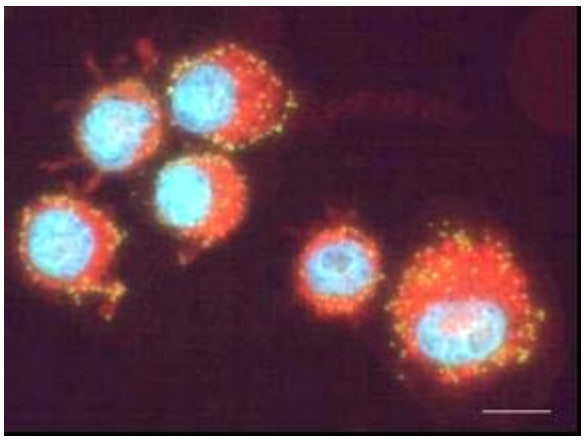

(b)

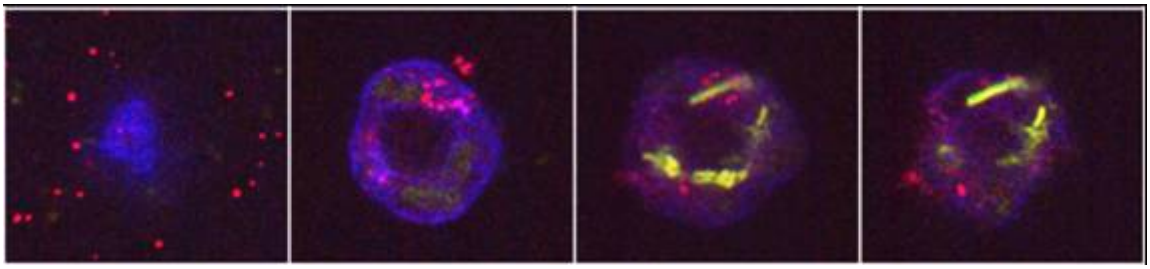

(c)

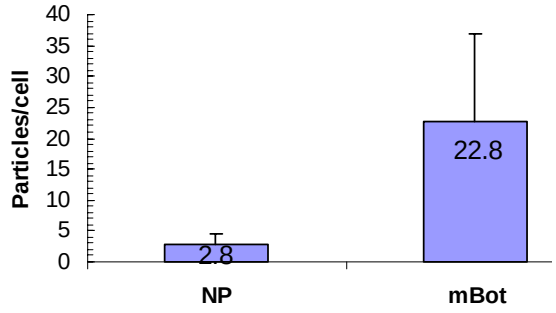

(d)

Supplementary Figure 6

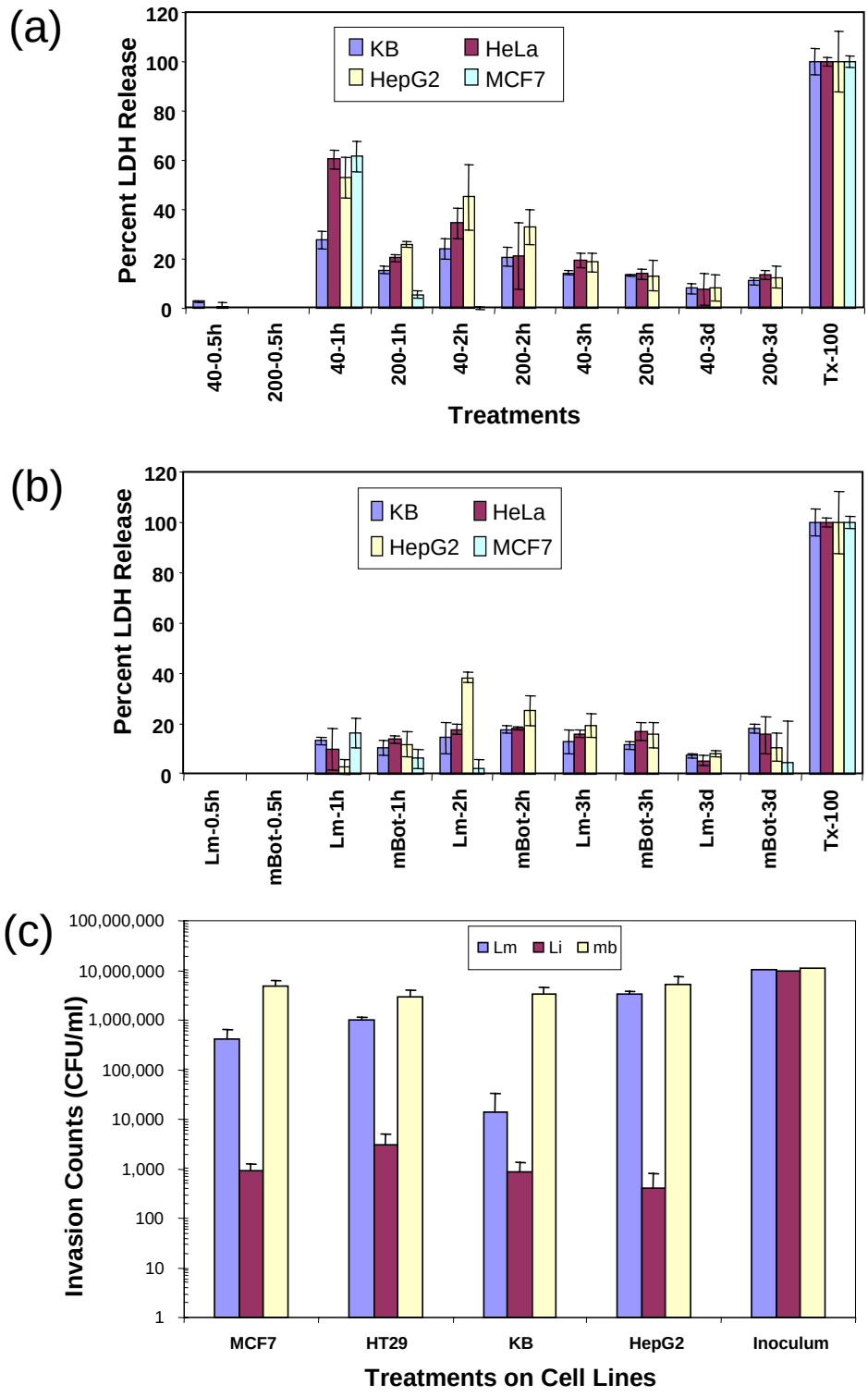

Supplementary Figure 7

References

[1]. Darji, A., Chakraborty, T., Niebuhr, K., Tsoins, N., Wehland, J., and Weiss, S. Hyperexpression of listeriolysin in the nonpathogenic species *Listeria innocua* and high yield purification. *J. Biotechnol.* **43**,205-212 (1995).

[2]. El-Agnaf, O. M. A., Jakes, R., Curran, M. D., Middletone, D., Ingenito, F., Bianchi, E., Pessi, A., Neill, D. & Wallace, A.. Aggregates from mutant and wild-type alpha-synuclein proteins and NAC peptide induce apoptotic cell death in human neuroblastoma cells by formation of beta-sheet and amyloid-like filaments. *FEBS Lett.* **440**, 71-75(1998).

[3]. Rasband, W.S., ImageJ, U. S. National Institutes of Health, Bethesda, Maryland, USA, http://rsb.info.nih.gov/ij/, 1997-2005.

[4] Zreiqat H, Sungaran R, Howlett CR, Markovic B. Quantitative aspects of an in situ hybridization procedure for detecting mRNAs in cells using 96-well microplates. *Mol. Biotechnol.* **10**, 107-113 (1998).

[5] Bouwer, H. G., Alberti-Segui, C., Montfort, M. J., Berkowitz, N. D., and Higgins. D. E. Directed antigen delivery as a vaccine strategy for an intracellular bacterial pathogen. *Proc. Natl. Acad. Sci. U S A.* **103**, 5102-5107 (2006).

[6] Angelakopoulos, H., et al. Safety and shedding of an attenuated strain of Listeria monocytogenes with a deletion of actA/plcB in adult volunteers: a dose escalation study of oral inoculation. Infect Immun. **70**, 3592-3601 (2002).

[7] Choi, H., Choi, S. R., Zhou, R., Kung, H. F., and Chen, I. W. Iron oxide nanoparticles as magnetic resonance contrast agent for tumor imaging via folate receptor-targeted delivery. *Acad Radiol.* **11**, 996-1004 (2004).